Observations of Mergers between Squall Lines and Isolated Supercell Thunderstorms

ADAM J. FRENCH* AND MATTHEW D. PARKER

Department of Marine, Earth, and Atmospheric Sciences, North Carolina State University, Raleigh, North Carolina

(Manuscript received 19 May 2011, in final form 23 November 2011)

ABSTRACT

A set of 21 cases in which an isolated supercell merged with a squall line were identified and investigated using analyses from the Rapid Update Cycle (RUC) model, archived data from the Weather Surveillance Radar-1988 Doppler (WSR-88D) network, and severe storm reports. This analysis revealed two primary environments associated with these mergers: a weak synoptic forcing, weak to moderate shear environment (WF) and a strong synoptic forcing, strong shear environment (SF). These environments bear a strong resemblance to those identified for progressive (WF) and serial (SF) derechoes in past studies. Radar reflectivity data revealed a spectrum of storm evolution patterns that generally lead to the merged system organizing as a bow echo. At one extreme, observed exclusively in the WF environment, the entire squall line evolved into a large bow echo following the merger. At the other extreme, observed for several cases in the SF environment, a localized bowing segment developed embedded within the larger squall line. The remaining cases exhibited characteristics best described as a hybrid of these extremes. Storm rotation generally weakened and became concentrated in low levels following the merger, although the exact evolution differed between the two background environments. Finally, an analysis of storm reports revealed that hail reports were maximized premerger and severe wind reports postmerger in both environments, while the distribution of tornado reports varied. In the WF environment a larger fraction of tornado reports occurred postmerger, while tornado production was maximized premerger in the SF environment. This suggests an evolving severe weather threat during the course of the merger, the details of which depend on the background environment.

1. Introduction

It has been observed that different organizational modes of convective storms tend to be associated with different severe weather threats (e.g., Gallus et al. 2008). Generally speaking, significant tornadoes and large hail often occur with supercell thunderstorms (e.g., Doswell and Burgess 1993; Davies-Jones et al. 2001) whereas widespread damaging straight-line winds are more frequently produced by linear modes, particularly bow echoes (e.g., Fujita 1978; Przybylinski 1995). In light of this, severe weather forecasters try to anticipate the predominant mode of organization that storms will take once they form, and how that mode may evolve over time. This can help them anticipate which severe weather hazards may occur and how those hazards may change with time. This becomes complicated, however, in cases where multiple organizational modes are present within a localized area (e.g., French and Parker 2008), especially when these modes merge into a single system. The present work seeks to improve our understanding of these situations, by investigating the effect that mergers between isolated supercells and squall lines have on storm organization and severe weather production.

Background

The majority of the past literature dealing with squall line–supercell mergers has consisted of observation-based analyses of individual cases, many of which produced significant tornadoes. Goodman and Knupp (1993) investigated a case from November 1989 wherein a merger between a squall line and an isolated supercell coincided with the development of a tornado rated F4 on the

* Current affiliation: South Dakota School of Mines and Technology, Rapid City, South Dakota.

Corresponding author address: Adam French, South Dakota School of Mines and Technology, 501 E. St. Joseph St., Rapid City, SD 57701.
E-mail: adam.french@sdsmt.edu

DOI: 10.1175/WAF-D-11-00058.1

Fujita scale that struck Huntsville, Alabama. Using regional composite radar data, observations from a nearby surface mesonet, and visual observations of the storm, the authors demonstrated that tornadogenesis appeared to coincide with an interaction between the supercell and the gust front associated with the squall line's cold pool. Furthermore, these observations also showed a ''distortion'' of the squall line's gust front, resulting from the merger. As the squall line approached the supercell, forward progress of its gust front slowed in the vicinity of the merger and accelerated south of the merger location, effectively appearing to ''wrap around'' the supercell's mesocyclone. This suggests that the supercell altered the structure of the squall line during the merger process. Additional studies also suggest a propensity for the supercell to play a dominant role in the merger process. Wolf (1998) analyzed what he described as the ''unexpected evolution'' of a merger between a supercell and bow echo that produced a large high-precipitation supercell, and continued to produce tornadoes for over an hour after the merger. Similar results were presented in Sabones et al. (1996) and Wolf et al. (1996), both of which documented interactions between squall lines or bowing line segments and supercells coinciding with tornadogenesis.

Squall-line–supercell mergers are not always associated with significant tornadoes, nor do they always promote sustained supercell structures. Several studies have also documented merger events that lead to the development of bow echoes. Fujita (1978) and Sieveking and Przybylinski (2004) both discussed cases where mergers between supercells and developing bow echoes appear to enhance the bow echo and produced widespread damaging winds. In these cases either little (Sieveking and Przybylinski 2004) or no (Fujita 1978) tornado damage was reported with the merged system. Additionally, Calianese et al. (2002) discussed a case where a merger between a bow echo and high-precipitation (HP) supercell produced significant flash flooding in the Dallas–Fort Worth, Texas, metro area, illustrating the variety of hazards posed by these merger events. All three of these cases exemplify events where the post-merger storm evolution closely resembled that commonly observed with bow echoes. It is not surprising that mergers between line segments and supercells lead to the development of bow echoes, as past work has shown that the often-observed evolution of HP supercells to bow echoes (e.g., Moller et al. 1990, 1994) may be related to storm mergers in the more general sense (e.g., Klimowski et al. 2004; Finley et al. 2001). In particular, Finley et al. (2001) found that enhanced precipitation following the merger strengthened the supercell's cold pool, leading to the development of the bow echo.

Thus, a review of previous works on the subject of squall-line–supercell mergers reveals a variety of outcomes that can produce a variety of severe weather threats. A broader examination of a larger number of cases seems warranted to develop an understanding of the common patterns of evolution associated with squall-line–supercell mergers, and what they mean for severe weather production. It would be useful to also further our understanding of storm evolution in cases where supercells merge with well-organized squall lines that are clearly larger in scale than the supercell. The present study looks to address both of these topics by examining a set of 21 cases wherein at least one supercell merges with a well-organized squall line.

Section 2 details the data and methods used in the study. In section 3 we introduce two common background environments associated with our merger cases, and discuss the convective organizations, and severe weather production associated with these environments. Finally, in section 4, we synthesize these results in light of past work and provide some concluding remarks and avenues for future study.

2. Data and methods

Candidate squall-line–supercell merger cases were initially identified using archived regional-scale composite radar reflectivity data maintained online by the Microscale and Mesoscale Meteorology (MMM) division at the National Center for Atmospheric Research (NCAR) (http://www.mmm.ucar.edu/imagearchive/). Data were reviewed from 2006 to 2010, focusing on the months of April, May, and June and the central United States (including the states of Texas, Oklahoma, Arkansas, Missouri, Iowa, Kansas, Nebraska, South Dakota, Colorado, and Wyoming). This time period was of interest so that we could make use of analyses from the 20-km horizontal-grid-spacing Rapid Update Cycle (RUC; Benjamin et al. 2004) mesoscale model, as detailed below. To be included, a case needed to contain persistent (present at a quasi-steady intensity for at least an hour prior to the merger), linear (defined as length-to-width ratio $> 5{:}1$), and isolated cellular structures that eventually merged. These cases were then further interrogated using single-site Weather Surveillance Radar 1988-Doppler (WSR-88D; Crum and Alberty 1993) reflectivity and radial velocity data in order to confirm that the individual cells identified were indeed supercells (e.g., contained a mesocyclone and relevant reflectivity structures such as hook echoes and/or weak echo regions), and that the two modes actually merged, which was not always clear given the coarser (approximately 15–30 min) temporal resolution of the composite data. A merger was defined as

a permanent union of the 40-dBZ radar reflectivity contours associated with the squall line and supercell. This resulted in 18 merger cases, which we supplemented with three additional cases from outside of the 2006–2010 date range in order to increase the sample size. These additional cases met all of the meteorological criteria for a merger, but occurred outside of the nominal geographic and temporal region outlined above. This increased the total to 21 cases, and a total of 29 merger events (due to some cases presenting multiple mergers; Table 1).

TABLE 1. Number of merger events categorized by convective organization (system-scale bowing, hybrid, embedded bowing, and other) and background environment. The total number of merger events is larger than the total number of cases owing to some cases producing multiple merger events.

Observed evolution	Weakly forced	Strongly forced
System-scale bowing	8	0
Hybrid	2	8
Embedded bowing	0	4
Other	2	5
Total merger events	12	17
Total cases	11	10

Our primary dataset for analysis was archived level II WSR-88D reflectivity and velocity data. For each case, data were obtained from all relevant radar sites to cover the duration of the event. These data were processed using the Warning Decision Support System-Integrated Information (WDSS-II; Lakshmanan et al. 2007) software developed collaboratively by the National Severe Storms Laboratory and the University of Oklahoma. The initial processing included quality controlling radar reflectivity to remove nonmeteorological echoes, dealiasing the radial velocity fields, and calculating azimuthal shear and radial divergence from the dealiased velocity data. WDSS-II uses a two-dimensional, local, linear least squares derivative technique to calculate these last two fields, which tends to be more tolerant of noisy data and is less dependent on a feature's position relative to the radar than other methods for calculating rotational and divergence signatures (Smith and Elmore 2004). The azimuthal shear data were then subjectively sorted to separate data associated with the premerger supercell, the premerger squall line, and the final merged system. This allowed us to calculate some statistics and time series data for the individual modes. Finally, to better facilitate comparison between cases, the reflectivity, dealiased velocity, and azimuthal shear data were interpolated onto constant-height grids, using the WDSS-II algorithm described by Lakshmanan et al. (2006). This was done to remove the range dependence of the height of the radar beam that occurs when viewing individual radar tilts and, thus, facilitate comparisons between cases where storms and mergers were at varying distances from the radar.

The hourly analysis fields from the RUC (Benjamin et al. 2004) forecast model were used to investigate the background environments associated with our merger cases. These data are desirable as they provide a complete three-dimensional picture of the atmosphere on an hourly time scale, as well as at 20-km horizontal grid spacing. This provides much higher spatial and temporal resolutions than can be found from observed radiosonde soundings alone. Furthermore, these data have been used extensively in the study of mesoscale phenomena, and found to have small errors when compared with available observations (e.g., Thompson et al. 2003; Benjamin et al. 2004). We used the RUC analyses to categorize each case based on its synoptic environment, as will be discussed in in section 3b. Prior to using these data, we qualitatively examined them for any apparent ''contamination'' due to unphysical simulated convective effects. While in some cases outflow boundaries associated with ongoing convection were present (as will be discussed in section 3b), we did not find any apparent signals of parameterized convection compromising these grids. To facilitate comparisons between cases, the RUC data for each case were first rotated so that the east–west axis was parallel to the mean squall-line motion over the 1-h time period centered on the merger. We then interpolated the rotated data onto a 1400 km $\times$ 1400 km grid (also with 20-km horizontal grid spacing) centered in time and space on the merger. These interpolated grids were used to examine individual cases and to create mean plots for the two primary synoptic environments discussed in the next section. For four cases, the 20-km RUC analyses were unavailable, and in their stead the analysis fields from the 40-km grid-spacing RUC model (two cases), and 32-km grid-spacing North American Regional Reanalysis [NARR; Mesinger et al. (2006); two cases] were used to characterize the background environments.

Finally, to evaluate the hypothesis that these types of merger events produce an evolving severe weather threat, we examined severe weather reports from the National Climate Data Center Storm Events Database associated with each of our cases. We subjectively sorted the reports, using radar data to identify which reports temporally and spatially corresponded to the premerger supercells, the premerger squall line (i.e., within approximately 50 km of the eventual merger location in the along-line direction), and the postmerger system (again, within 50 km along the squall line of the merger location). Reports from nearby storms not involved in the merger were excluded. The report times were converted to a merger-relative time framework (i.e., minutes

before or after the onset of the merger) to facilitate comparison between cases. The limitations to the storm events dataset have been well documented in the literature (e.g., Doswell and Burgess 1988; Witt et al. 1998; Weiss et al. 2002; Doswell et al. 2005; Verbout et al. 2006; Trapp et al. 2006); however, this dataset still remains the most complete source of data of this type. We will address some of these specific limitations, and our attempts to lessen their impact on our results, in section 3e.

3. Results

a. Overview

One of the primary goals of investigating a large number of cases was to try to find commonalities associated with these types of squall-line–supercell merger events. In reviewing the single-site radar reflectivity data, we found that in an overwhelming majority of the merger events (22 of the 29 identified) the postmerger evolution was characterized by the development of some type of bow echo (Fujita 1978) structure (the system-scale bowing, hybrid, and embedded bowing rows in Table 1). The remaining cases (the ''other'' row in Table 1) showed a variety of patterns of evolution, ranging from the supercell being absorbed into the squall line and dissipating, to the merged system evolving into a large supercell. While the evolution toward bow echoes was a common occurrence, we found that rather than falling into clear evolutionary archetypes, these events instead tend to fall within a spectrum of convective evolutions, as will be discussed in section 3c. We found it more informative, and deemed it potentially more useful in the forecasting sense, to organize our cases based upon the characteristics of their background environments. Cases were subjectively grouped based on the strength of the synoptic-scale forcing, similar to the method of Evans and Doswell (2001) and could be classified by one of two general environments: a weakly forced (WF) synoptic environment characterized by a low-amplitude 500-hPa trough and a weak or nonexistent surface cyclone in the vicinity of the merger, and a strongly forced (SF) synoptic environment characterized by a high-amplitude 500-hPa trough, and a mature surface cyclone in the vicinity of the merger. This classification scheme resulted in 11 WF cases (the weakly forced column in Table 1) and 10 SF cases (the strongly forced column in Table 1). The details of these environments are presented in the next section.

b. Background environment

The mean WF environment at the time of merger is characterized by a low-amplitude 500-hPa short-wave trough to the west of the merger location, with a 15–20 m s^{-1} wind maximum over the merger location (Fig. 1a). The primary surface feature is a weak warm front oriented nearly parallel to the squall-line motion extending through the merger location (Fig. 2a). Also notable is the absence of a deep surface cyclone and attendant cold front. These mean surface features were consistent with observations from many of the individual cases, as the merger occurred near or along a warm front in six of the cases analyzed (Figs. 3a,c,d,f,g,h), while cold fronts or drylines were only present in four cases, primarily well away from the merger (Figs. 3c,d,g,h). Given the proximity of these storms to the warm front, it is possible that they were at least partially feeding on air from the cold side of the boundary; however, the presence of cold pools evident in surface observations and RUC data (e.g., Figs. 3b,g,h) leads us to believe that many of these storms remained surface based, at least through the merger process. The details of the upper-air patterns associated with these cases were considerably more variable than the surface pattern (e.g., Fig. 3), which accounts for the larger standard deviation in the mean plot (Fig. 1c). These patterns ranged from a closed low (e.g., Fig. 3d) to zonal flow (e.g., Fig. 3f), but the common characteristic was the generally weak upper-level troughing, implying weak synoptic forcing.

All told, this synoptic pattern bears a strong resemblance to the to the ''progressive derecho'' environment identified by Johns and Hirt (1987), and the ''warm season'' bow-echo environment discussed by Johns (1993), both of which were characterized by warm fronts at the surface and a weak upper-level synoptic forcing. These types of environments favor long-lived, isolated bow echoes, that are primarily cold-pool driven rather forced along a synoptic boundary. Notably, there is evidence of large cold pools in the RUC data for three of our WF cases (Figs. 3b,g,h), consistent with what is expected for weaker synoptic forcing.

In contrast to the WF environment, the mean SF environment is characterized by a high-amplitude 500-hPa trough west of the merger with a 30 m s^{-1} upper-level jet impinging on the merger location (Fig. 1b). Accordingly, a strong surface cyclone was also present, with the mean merger location in the warm sector just ahead of the ''triple point'' intersection of the dryline and the cold and warm fronts (Fig. 2b). This matches well the merger occurring in the warm sector, ahead of the triple point in most of the SF cases (Figs. 4b,c,d,e,f,g,h), although slight differences in the exact location of the low pressure center and boundaries resulted in the comparatively large standard deviations in Fig. 2c. The presence of the cold front and dryline appeared to be important to the development of the squall line in these cases, as analysis of

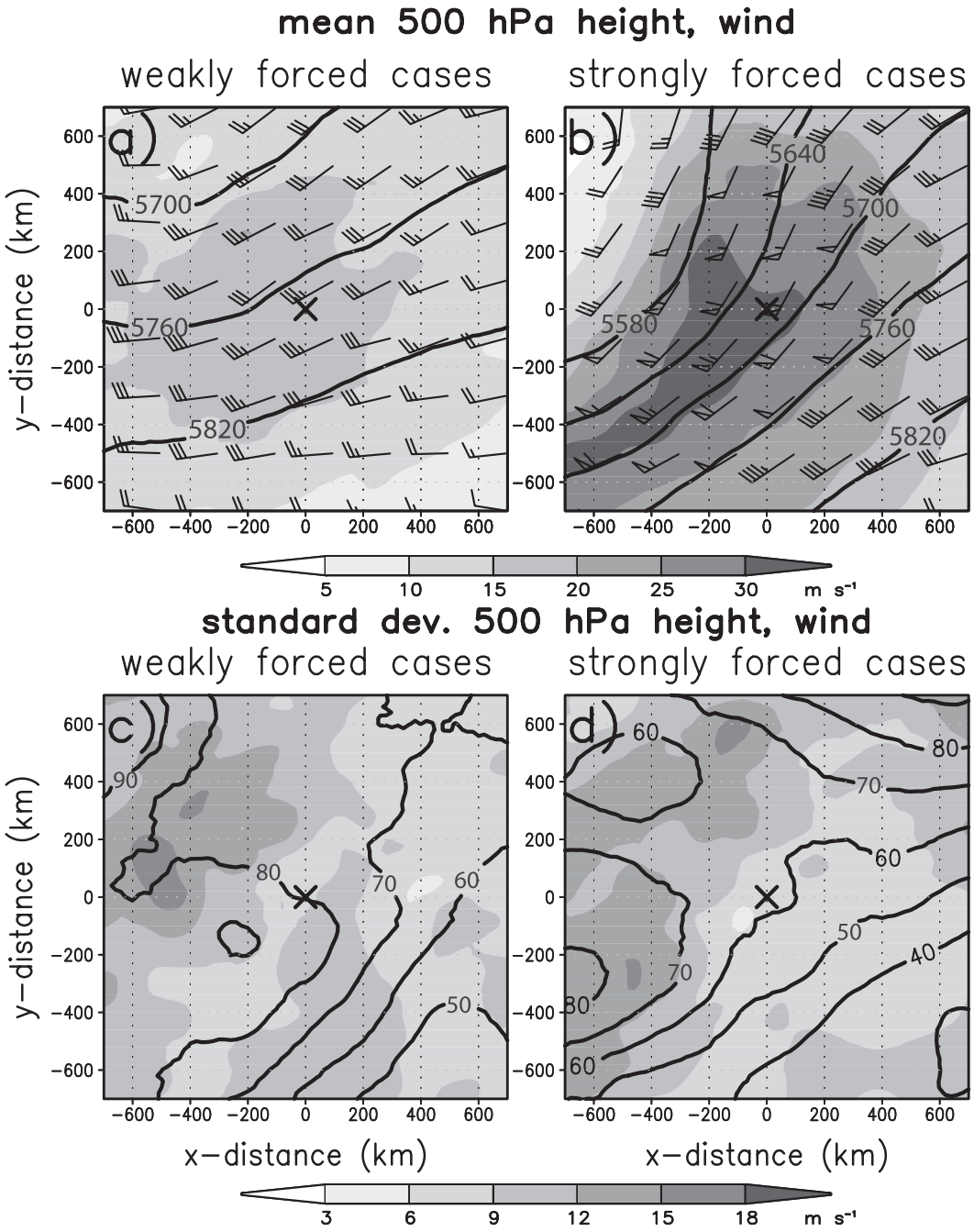

FIG. 1. Mean RUC analysis 500-hPa height (m, contours) wind barbs (m s^{-1}; half barb = 2.5 m s^{-1}, full barb = 5 m s^{-1}, flag = 25 m s^{-1}), and wind speed (m s^{-1}, shaded as shown) for the (a) WF and (b) SF environments. Standard deviation of the 500-hPa height (contours, m) and wind speed (shaded, m s^{-1}) for the (c) WF and (d) SF environments. The black × in each panel marks the mean merger location.

surface observations and radar finelines (not shown) often revealed the squall line developing along the cold front. In several cases the squall line was observed to develop quite rapidly in the region where the cold front was overtaking the dryline (e.g., Figure 4b,d,f). The supercells in these cases typically developed prior to the squall line, often originating along the dryline and then moving into the warm sector. This is similar to the findings of French and Parker (2008), who found that variations in forcing strength played a role in triggering a squall line and a group of supercells in a nonmerger multimode case.

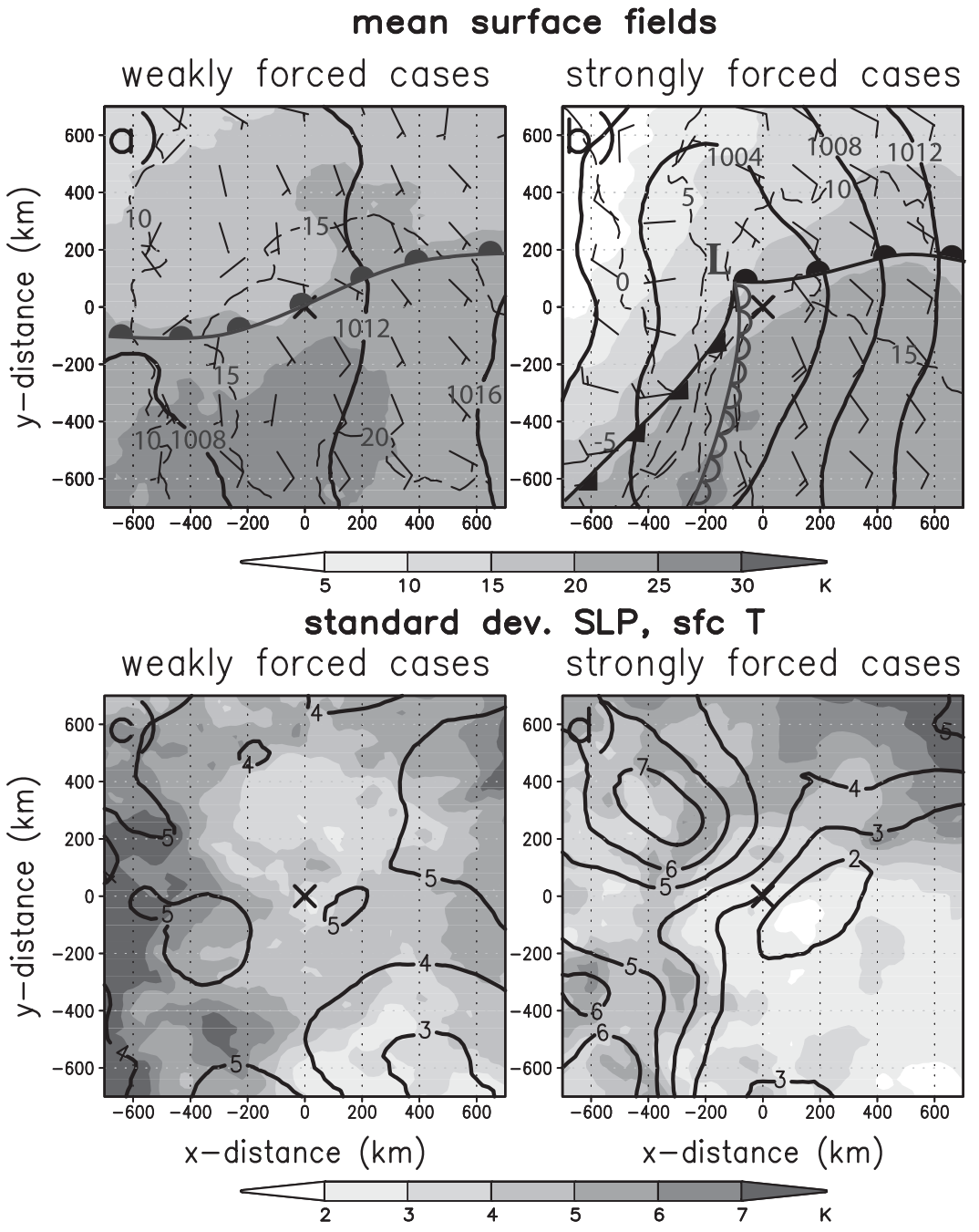

FIG. 2. Mean RUC analysis sea level pressure (hPa, solid contours), surface temperature (°C, shaded as shown), dewpoint temperature (°C, dashed contours), and 10-m AGL winds (m s^{-1}, wind barbs as in Fig. 1) for the (a) WF and (b) SF environments. Standard deviation of sea level pressure (hPa, contours) and surface temperature (°C, shaded as shown) for the (c) WF and (d) SF environments. The black × in each panel marks the mean merger location.

This synoptic environment is quite similar to the ''serial derecho'' pattern of Johns and Hirt (1987) and the ''dynamic'' bow-echo environment of Johns (1993). Particularly, the strong linear surface forcing along the cold front suggests an environment more favorable for comparatively longer squall lines with embedded bowing segments, rather than a single, large bow echo. In addition, as noted by Johns (1993), this environment shares a number of similarities with the ''classic'' Great Plains tornado outbreak pattern, which would suggest that sustained supercell structures may also be favored.

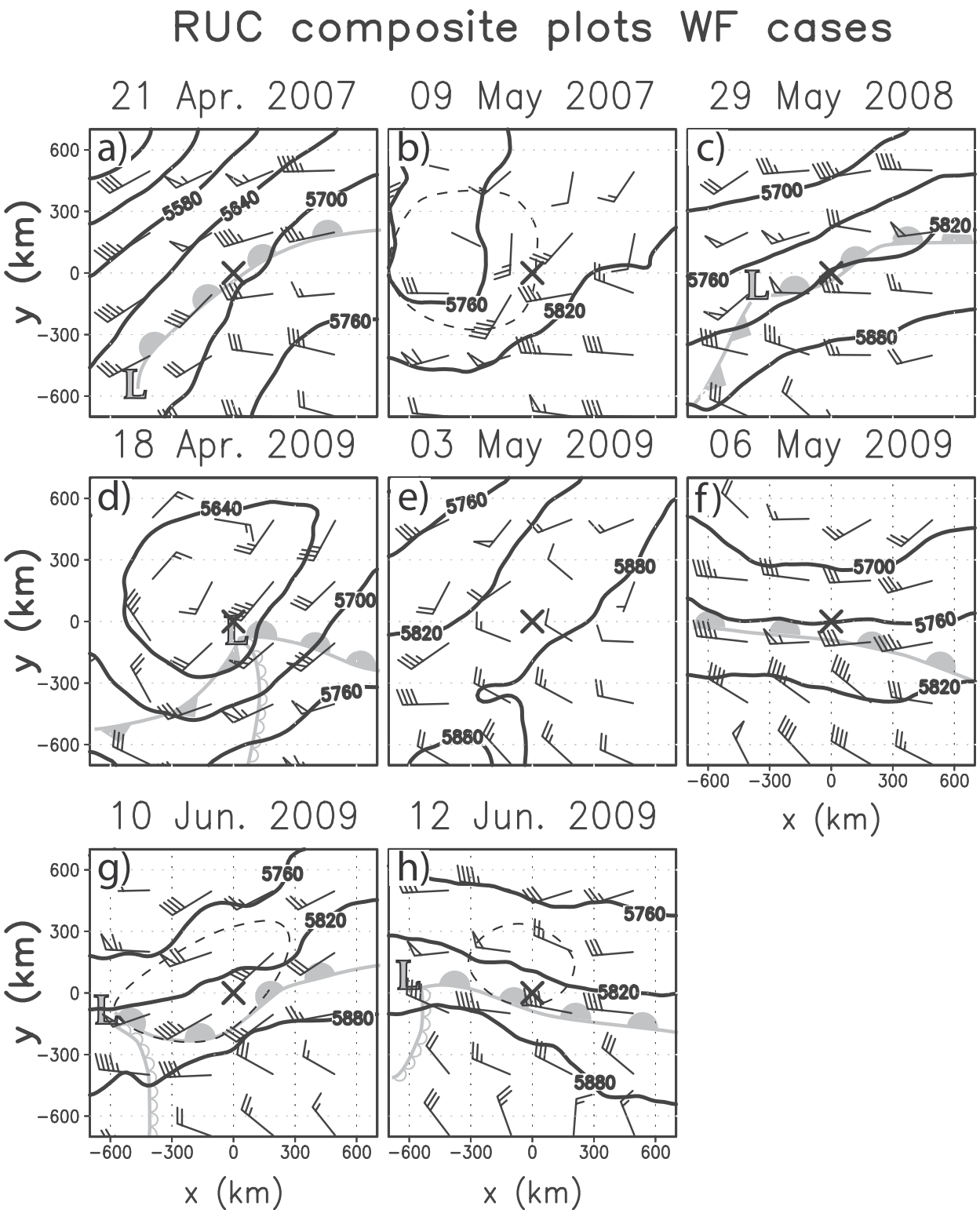

FIG. 3. (a)–(h) Environmental parameters from RUC analysis data associated with the WF cases. Plotted fields include 500-hPa height (m, black contours), 0–6-km shear vector (m s^{-1}, wind barbs as in Fig. 1), and locations of surface low pressure center, warm fronts, cold fronts, and drylines, using traditional notation. The dashed lines in (b), (h), and (i) denote cold pools associated with the squall line present in the RUC analysis. The black × in each panel marks the merger location.

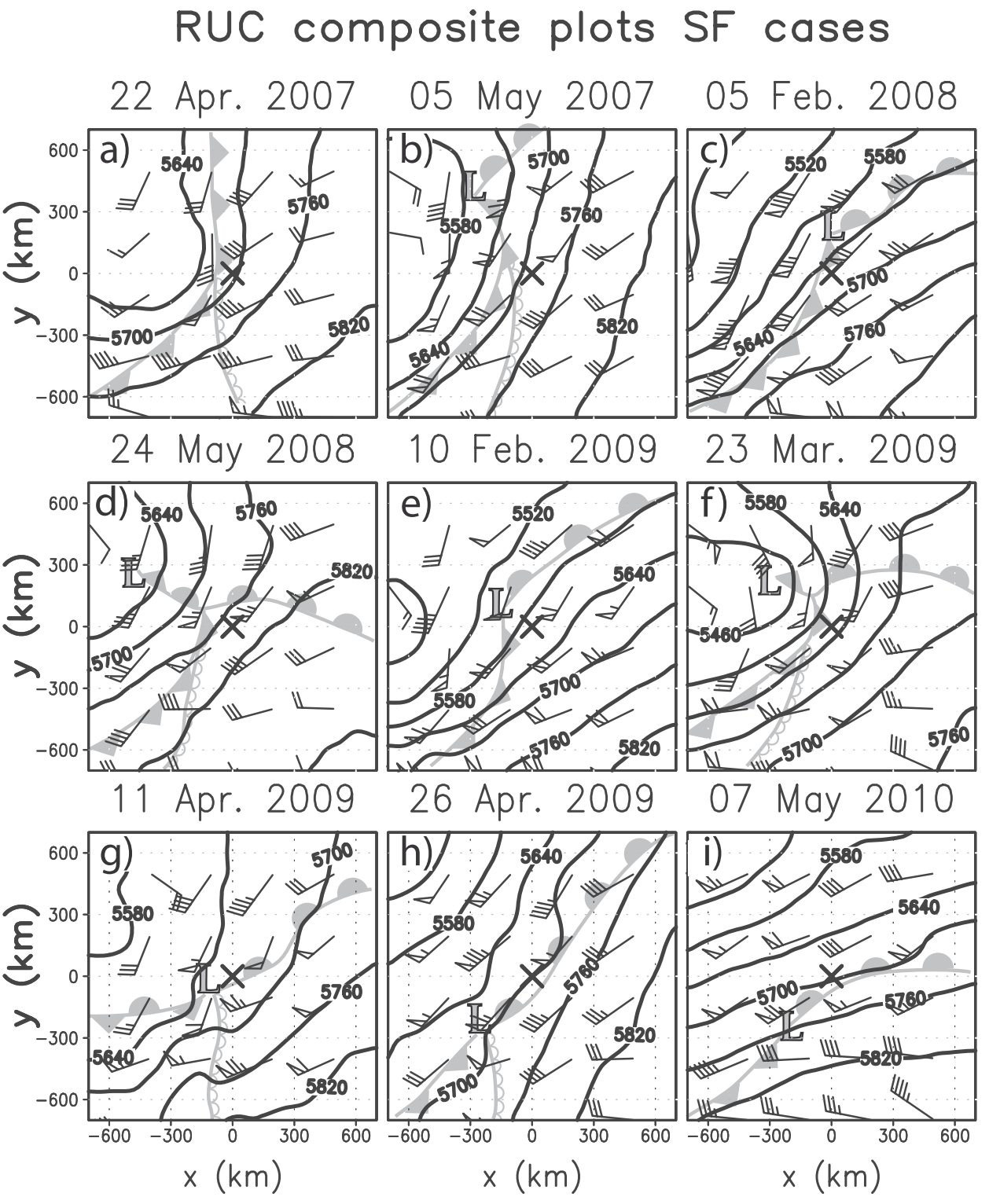

FIG. 4. As in Fig. 3, but for SF cases.

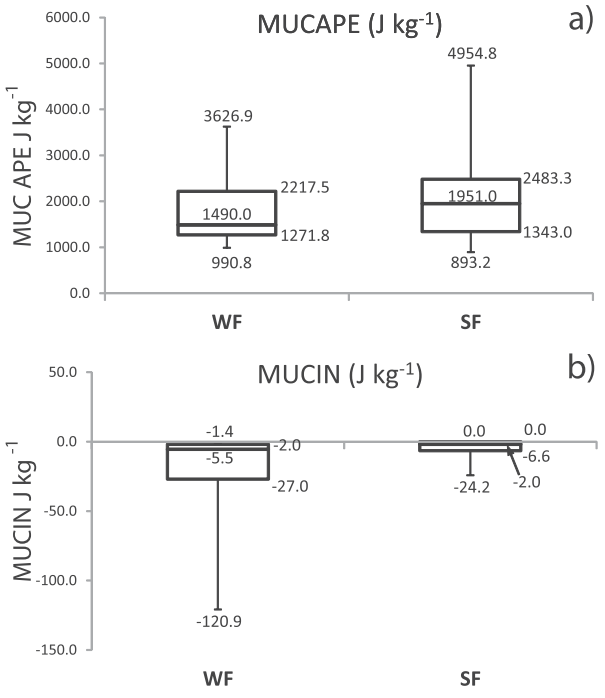

FIG. 5. Box-and-whiskers plots of (a) MUCAPE (J kg^{-1}) and (b) MUCIN (J kg^{-1}). Boxes denote the 25th–75th percentiles, with the horizontal line inside the box indicating the median value. Vertical lines (whiskers) extend to the 10th and 90th percentiles.

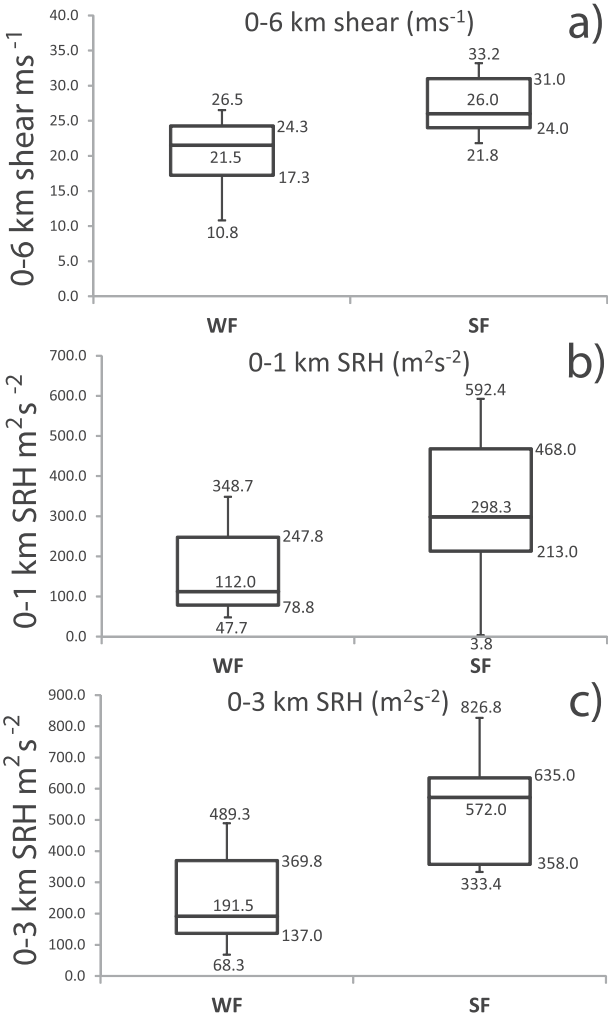

FIG. 6. As in Fig. 5, but for (a) 0–6-km AGL bulk wind shear (m s^{-1}), and (b) 0–1- and (c) 0–3-km AGL SRH (m^2 s^{-2}).

As a final comparison of the WF and SF environments, some common severe weather parameters were computed from near-merger proximity soundings created for each case using the RUC data (Figs. 5 and 6). The two environments were quite similar thermodynamically, with median most unstable convective available potential energy (MUCAPE) values differing by only 500 J kg^{-1} and a good deal of overlap between the interquartile ranges (Fig. 5a). The most unstable convective inhibition (MUCIN) was similar for both environments (Fig. 5b), although the WF environment skewed toward slightly larger values owing to several cases where the merger occurred along a warm front rather than in the warm sector (e.g., Figs. 3a,c,f,g,h). Parameters related to the vertical wind shear more clearly differentiated the environments, as the SF environment contained larger 0–6-km shear (Fig. 6a), 0–1-km storm-relative helicity (SRH; Fig. 6b), and 0–3-km SRH (Fig. 6c). All told, this suggests that the SF environment more strongly favors supercells (large 0–6-km shear and 0–3-km SRH) and possibly tornadoes [large 0–1-km SRH, e.g., Rasmussen and Blanchard (1998); Thompson et al. (2003)]. The deep-layer shear values in the WF environment were generally toward the lower end expected for supercells (17–24 m s^{-1}; Fig. 6a), but within the range commonly observed for echo organizations (Doswell and Evans 2003). However, for many of the cases the 0–3-km SRH was sufficient to support supercells (Fig. 6c), suggesting the low-level shear may have been more important in these cases. Given that many of the WF mergers occurred along a warm front, we hypothesize that the high-SRH air located along the frontal boundary may have been important in sustaining supercells structures in this environment (e.g., Markowski et al. 1998). The median 0–1-km SRH for the WF environment (Fig. 6b) was less than that generally observed for tornadic supercells (Thompson et al. 2003), suggesting a lower likelihood of tornadic storms in this environment.

To summarize, the mean WF environment was characterized by a weak upper-level trough, and the merger tended to occur along a warm front. These cases generally had 0–6-km bulk shear toward the lower end of

the range observed for supercells, with sufficient SRH to support supercells, but not necessarily tornadoes. On the other hand, the mean SF environment was characterized by a deep upper-level trough west of the merger, which usually occurred in the warm sector of a surface cyclone in the vicinity of the triple-point intersection of the surface boundaries. The vertical wind shear and storm relative helicity were generally much larger in this environment, favoring supercell structures, and potentially tornadoes. Notably, the mean synoptic features associated with the WF and SF environments (e.g., Figs. 1 and 2) share many similarities to those commonly associated with different organizations of bow echoes (Johns and Hirt 1987; Johns 1993). In particular, the background synoptic pattern and vertical wind shear in the WF environment would traditionally favor large, isolated bow echoes, while the synoptic pattern and vertical wind shear in the SF environment are more favorable for large squall lines with embedded bowing segments. As will be shown next, these expected squall-line organizations are very similar to the observed postmerger storm morphologies in the WF and SF environments.

c. *Reflectivity analysis*

As mentioned earlier, the reflectivity structures associated with these merger events can best be described as covering a spectrum of convective patterns of evolution that frequently produce bow-echo structures (Table 1). At one extreme, after the merger, the entire squall line evolved into a large bow echo, as illustrated in Fig. 7a and the example in Figs. 8a–e. We have termed this evolution system-scale bowing (SSB). It was observed exclusively in the WF environment and was the most common evolution in that environment (Table 1). In these cases, the squall line and supercell tend to have similar directions of motion (Fig. 7a, $t = 1$) and the merger typically results from the squall line overtaking the supercell. As it approaches the supercell, the squall line tends to slow its eastward progress and weaken north of the eventual merger location[1] (Fig. 7a, $t = 2$). The squall line typically merges with the rear flank of the supercell, leading first to a Y-shaped echo (as the forward-flank precipitation associated with the supercell continues to extend eastward from the squall line; Fig. 7a, $t = 3$; Fig. 8c). On average, the merger process itself (i.e., the time between the initial union of 40-dBZ echo and the supercell becoming completely merged with the squall line) takes approximately 25 min for the SSB evolution. As the merger progresses, it is associated with an increase in radar reflectivity values near and south of the merger location, and the squall line begins to take on an S shape (Fig. 7a, $t = 4$; Fig. 8d). Eventually a swirl pattern becomes evident near the north end of the squall line and the bowing becomes more pronounced (Fig. 7a, $t = 5$). By this point, the merger location–remnant supercell now represents the north end of the squall line, and any remaining radar echoes north of this point have weakened considerably. Typically, a large comma-shaped echo (Fujita 1978) emerges as the bowing structure becomes most evident within 1–2 h following the merger (Fig. 7a, $t = 6$; Fig. 8e).

This pattern of evolution typically occurs in cases where a single supercell was present and merged with the squall line, and the postmerger evolution appears similar to that detailed in several past studies (e.g., Fujita 1978; Sieveking and Przybylinski 2004). Additionally, there are a number of qualitative similarities between the reflectivity structures in the SSB evolution, and those associated with the often-observed high-precipitation supercell–bow-echo transition (e.g., Moller et al. 1990; Moller et al. 1994). This includes the development of strong bowing south of the remnant supercell circulation and the presence of swirl patterns in the reflectivity field that appears to be associated with this circulation. That the SSB evolution was the preferred outcome in the WF environment is not surprising, as this environment strongly resembles one associated with large bow echoes [e.g., the progressive derecho of Johns and Hirt (1987) and Johns (1993)]. What is less clear is the degree to which the merger facilitates or accelerates bow-echo development in these cases. While it would be tempting to conclude that there was a direct causal effect given the temporal connection between merger and bow-echo development in a number of these case, the present data are insufficient to make such an assessment. Seeing as the squall lines in a number of SSB cases exhibited varying degrees of bowing prior to the merger (e.g., Fig. 8b), it is likely that the favorable environment may play an important role in the development of bowing structures in these cases. The relative contributions of background environment and the merger–bow-echo development are currently being investigated using idealized model simulations, and will be the subject of a future manuscript.

At the other end of the evolutionary spectrum, we observed what we have termed embedded bowing (EMB). In these cases, following the merger, a small-scale bowing segment develops along the squall line but the entire line does not evolve into a bow echo (Figs. 7b, 8f–j). This evolution was only observed in the SF environment, in four cases total (Table 1). In these situations the supercell

[1] For the sake of simplicity, we will assume an eastward-moving squall line oriented north–south, as shown in the schematic in Fig. 7.

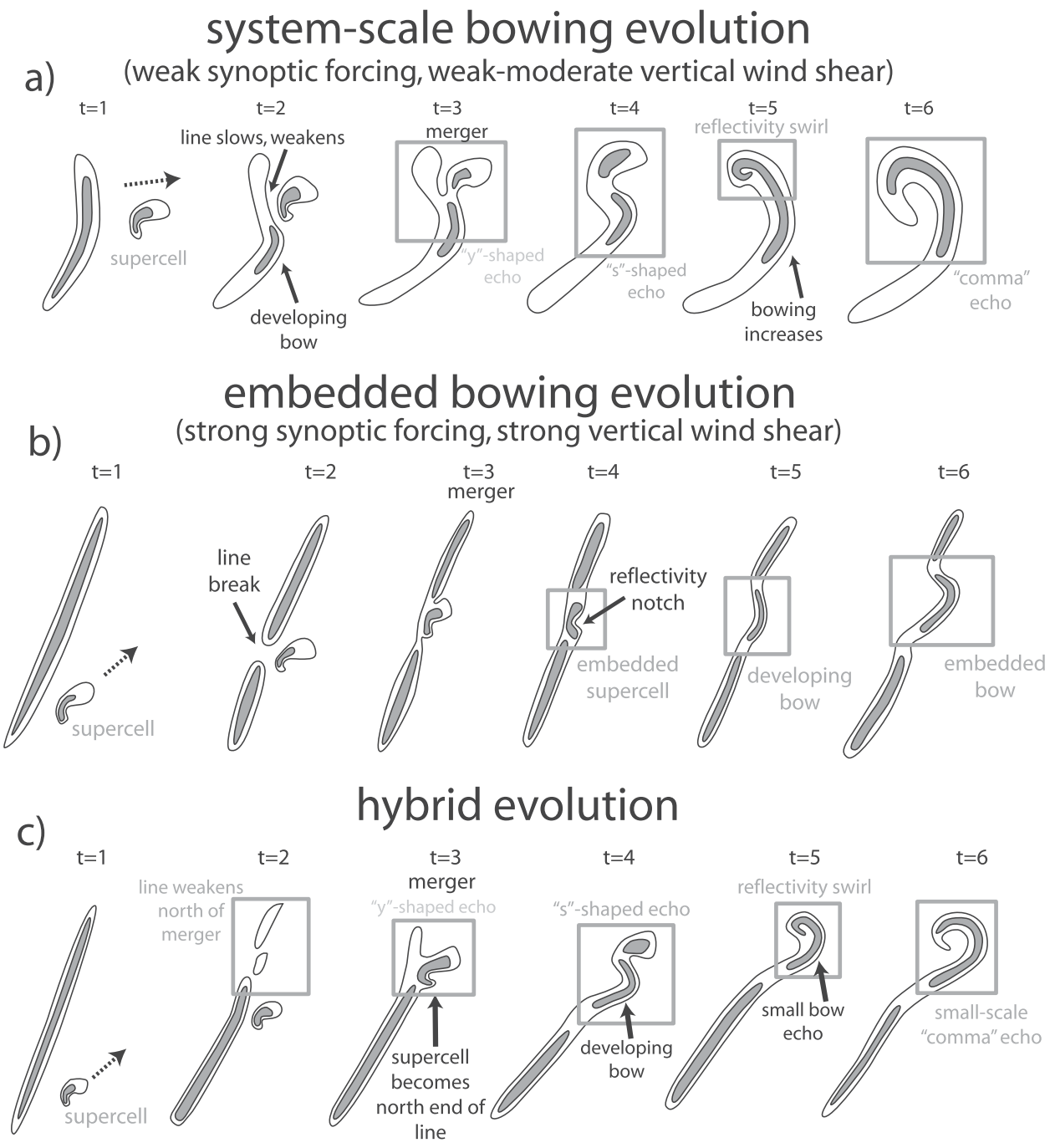

FIG. 7. Schematic diagrams illustrating the (a) system-scale bowing, (b) embedded bowing, and (c) hybrid evolutions as they would appear on radar (gray shading denotes higher radar reflectivity values). The dashed arrows at $t = 1$ represent initial supercell motion vectors.

typically has a direction of motion that is largely parallel to the squall line's major axis (Fig. 7b, $t = 1$). As the squall line approaches, it typically weakens or "breaks" in the vicinity of the supercell (Fig. 7b, $t = 1$–2; Fig. 8g). The forward flank of the supercell then will merge first at the northern end of this break, followed by the rear flank of the supercell merging with the line south of the break (Fig. 7b, $t = 3$; Fig. 8h). Similar to the SSB evolution pattern, this process takes approximately 20 min on average in the EMB cases. Following the merger, the supercell remains evident as an embedded structure within the squall line, typically characterized by a notchlike feature within the

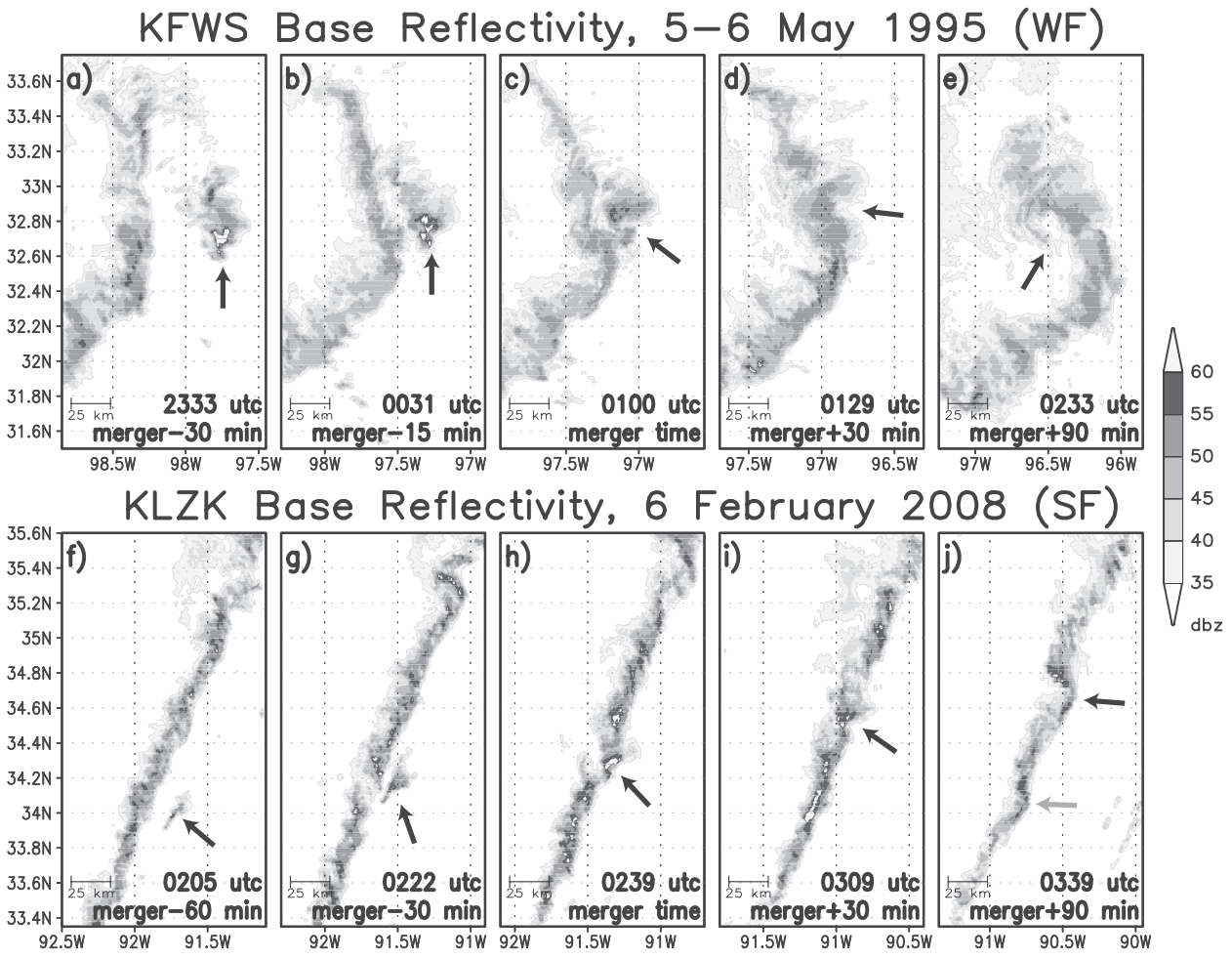

FIG. 8. Examples of (a)–(e) the system-scale bowing evolution in a WF environment and (f)–(j) the embedded bowing evolution in an SF environment. Data are WSR-88D 0.5° tilt radar reflectivities from (a)–(e) Fort Worth (KFWS) between 2333 5 May and 0233 6 May 1995 and (f)–(j) Little Rock, AK (KLZK), between 0205 and 0339 UTC 5 Feb 2008. Arrows denote the isolated supercell–merged system or other features of interest described in the text.

line (Fig. 7b, $t = 4$; Fig. 8h–i). Eventually, this feature evolves into a small-scale bow echo embedded within the larger line, sometimes also exhibiting reflectivity swirl features as discussed for the SSB evolution above, albeit on a smaller scale (Fig. 7b, $t = 5$–6; Fig. 8j). The whole process from initial merger to embedded bowing structure can take upward of 1–2 h and thus influence the local organization of the squall line well after the merger occurs.

The EMB cases often occur in situations where multiple supercells are present ahead of a comparatively long squall line, and thus multiple mergers can occur within a single case leading to a line-echo wave pattern (LEWP; Nolen 1959) organization of the squall line. It should also be noted that in these cases there were often additional bowing structures present away from the merger (i.e., the gray arrow in Fig. 8j). Thus, it would appear that in the EMB cases the merger was not a necessary condition to get a bowing segment, but it still may have served as a catalyst to promote bowing at a particular location along the squall line. Additionally, it makes sense that the EMB evolution was observed exclusively in the SF environment as this environment is very similar to that commonly associated with LEWP-type squall lines [e.g., the serial derecho of Johns and Hirt (1987) and Johns (1993)]. Thus, as in the SSB evolution, the postmerger in the EMB cases appears to be strongly governed by the background environment as well.

While the SSB and EMB evolution patterns represent the extremes on the spectrum of postmerger organizations, many cases contained features common to both of these evolutions and are, thus, best described as a hybrid of the two (Fig. 7c). We found examples of this type of evolution in both the WF and SF environments (e.g., Figs. 9a–e and 9f–j, respectively), although it was more

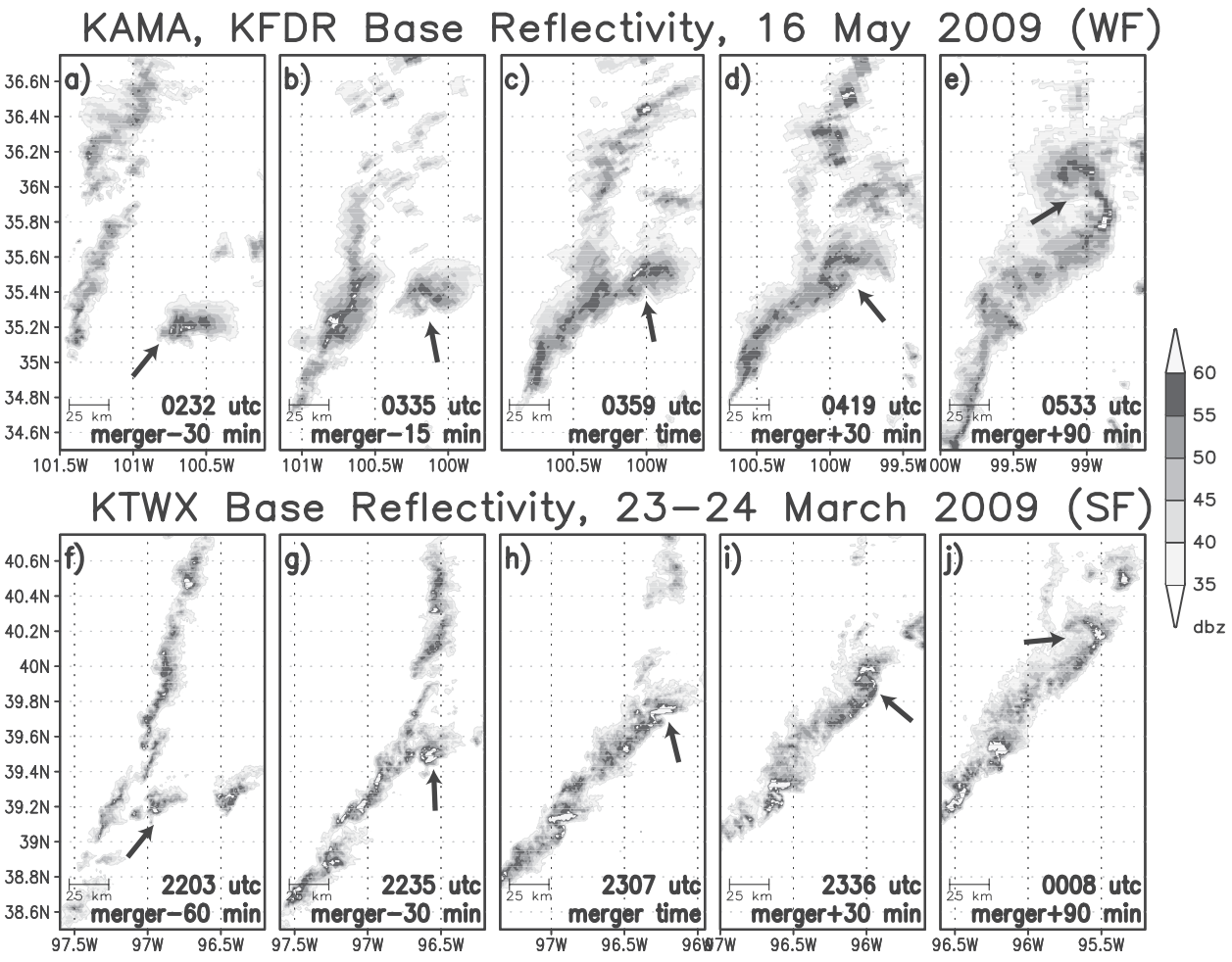

FIG. 9. Examples of the hybrid evolution in (a)–(e) a WF environment and (f)–(j) an SF environment. Data are WSR-88D 0.5° tilt radar reflectivities from (a) Amarillo, TX (KAMA), at 0302 UTC 16 May 2003; (b)–(e) Frederick, OK (KFDR), from 0335 to 0533 UTC 16 May 2003; and (f)–(j) Topeka, KS (KTWX), between 2203 UTC 23 Mar and 0008 UTC 24 Mar 2009. Arrows denote the isolated supercell/merged system or other features described in the text.

common in the SF environment, representing the most frequently observed evolution in that environment (Table 1). These cases often begin with a large squall line, as in the EMB evolution (Fig. 7c, $t = 1$); however, as the supercell approaches, the line weakens and ultimately dissipates to the north of the merger point (Fig. 7c, $t = 2$; Figs. 9a–c and 9g–h). Similar to the SSB evolution, the merger process (formation of the permanent 40-dBZ union) takes approximately 25 min for the hybrid cases. As the supercell merges, it becomes the north end of the squall line, proceeding through the Y- and S-shaped patterns of the echo evolution common to the SSB evolution (Fig. 7c, $t = 3$–4; Figs. 9c–d and 9h–i) and eventually developing a small-scale bow and comma echo (Fig. 7c; $t = 5$–6; Figs. 9e,j). The primary difference, however, is that the resultant bow remains similar in scale to the merged supercell, and while the line may reorient south of the merger, it does not evolve into a large bow echo, as seen in the SSB cases (cf. Figs. 7a,c, $t = 3$–6). In fact, in some cases additional embedded bowing segments are observed away from the merger location, not unlike what is observed in the EMB cases, and in several cases multiple mergers occurred and followed the hybrid evolution. While the observation of this evolution in both the WF and SF environments implies that the background environment is not the primary control, it still appears to play an important role. The hybrid cases observed in the WF environment appeared closer to the SSB end of the spectrum (cf. Figs. 8a–e and 9a–e), while those observed in the SF environment had more similarities with the EMB evolution (cf. Figs. 8f–j and 9f–j). Thus, for a given environment the delineation between the SSB or EMB and hybrid evolutions may ultimately come down to storm-scale details such as the

relative size or maturity of the squall line–supercell or the relative location of the merger. For instance, both the SSB and hybrid evolution patterns appear to follow from mergers that occur near the north end of the line, while the EMB evolution follows mergers that occur near the middle of the squall line. The relative importance of merger location is currently being investigated using idealized numerical simulations, the results of which will be reported upon in a future paper.

To summarize, the overwhelming majority of the merger cases that we examined produced an ultimate storm organization that resembled a bow echo. The behavior ranged from the development of a large bow echo (the SSB evolution), seen in most of the WF cases, to a small-scale bowing segment embedded within a larger line (the EMB evolution) seen in several SF cases. The remaining cases, primarily in the SF environment, evolved as a hybrid of these extremes. These patterns of evolution are consistent with those of nonmerger bow echoes observed for similar weakly and strongly forced environments by Johns and Hirt (1987) and Johns (1993). In these studies, large-scale bow echoes [i.e., the progressive derecho of Johns and Hirt (1987, their Fig. 3)] tended to be associated with more weakly forced events, while lines with smaller-scale embedded bow echoes [i.e., the serial derecho of Johns and Hirt (1987, their Fig. 6)] were associated with strongly forced events.

d. Velocity analysis

In addition to examining the reflectivity features associated with squall-line–supercell merger events, we were also interested in examining what happens to the velocity signatures associated with these two modes when the merger occurs. Specifically, how does the existing mesocyclone associated with the supercell evolve as the merger takes place, and what influence might this have on subsequent storm organization? To facilitate comparison among multiple cases, we focused our analysis on azimuthal shear calculated from the dealiased radial velocity data as a means of identifying and tracking rotational features. As discussed in section 2, these data were interpolated to a three-dimensional grid and subjectively sorted, so that only those data associated with the premerger supercell and merged system were evaluated.

One of the most basic questions pertaining to the evolution of the supercell's mesocyclone in these cases is whether or not it remains evident following the merger (i.e., does the mesocyclone persist within the merged system?). To address this question, we tracked azimuthal shear values over time associated with each supercell and its subsequent merged system. This was done both by looping images, and looking at plan-view plots of the accumulated azimuthal shear over time to produce rotation tracks associated with these features (e.g., Fig. 10). In most cases, the rotational signature initially associated with the supercell could be tracked in a linear fashion following the merger. The exact evolution of the rotational features postmerger varied considerably, with azimuthal shear weakening (e.g., Figs. 10b,d), remaining constant (Fig. 10c), or intensifying (Fig. 10a) after the merger depending on the case. Additionally the direction of the rotation tracks varied after the merger as well, although most cases either saw little change in the path of rotation (approximately 50% of cases; e.g., Figs. 10b,d), or a turn to the right relative to the initial supercell motion (approximately 36% of cases; e.g., Figs. 10a,c). Most of the cases exhibiting no change in direction occurred in the SF environment, while examples in both environments were found that turned to the right. We interpret this as representing two different avenues for supercell behavior postmerger. The cases where the rotation track is largely unchanged indicates a sustenance of supercell features postmerger, as the storm does not appear to be disrupted or altered by the squall line. This is consistent with the embedded supercell period of the evolution seen in some of the SF cases (e.g., the EMB evolution; Fig. 7b, $t = 4$). The cases where there is a pronounced turn to the right likely indicate that the supercell has acquired a motion vector similar to the squall line's, suggesting that the squall line is playing a dominant role in the merger in these cases. Which supercell pathway occurs may depend on the storm-scale details of a given event, including the strength of the squall line's cold pool.

To better understand the details of the evolution of rotation features associated with the merger case, the maximum azimuthal shear associated with the supercell, and eventual merged system was examined over time and height for each merger case. From the example WF cases shown in Fig. 11, it is clear that the details of this evolution vary from case to case; however, there are some common features that stand out. In most of the WF cases, azimuthal shear is observed to weaken around the time of merger ($t = 0$ in Figs. 11a–f). For some cases this occurs just after the merger (e.g., Figs. 11a,b,d), while in other cases it appears to precede, or occur coincident with, the merger (e.g., Figs. 11c,e,f). Following this initial decline in rotation around the merger time, a subsequent reintensification of rotation was often observed (e.g., Figs. 11a,c,d,e,f). Generally, this reintensification was concentrated in lower levels than the premerger supercell rotation (e.g., generally below 3 km AGL; Figs. 11a,c,d,f), although in some cases a strong, deep, rotational feature developed (Fig. 11e). We interpret the initial decline in azimuthal shear as resulting from a

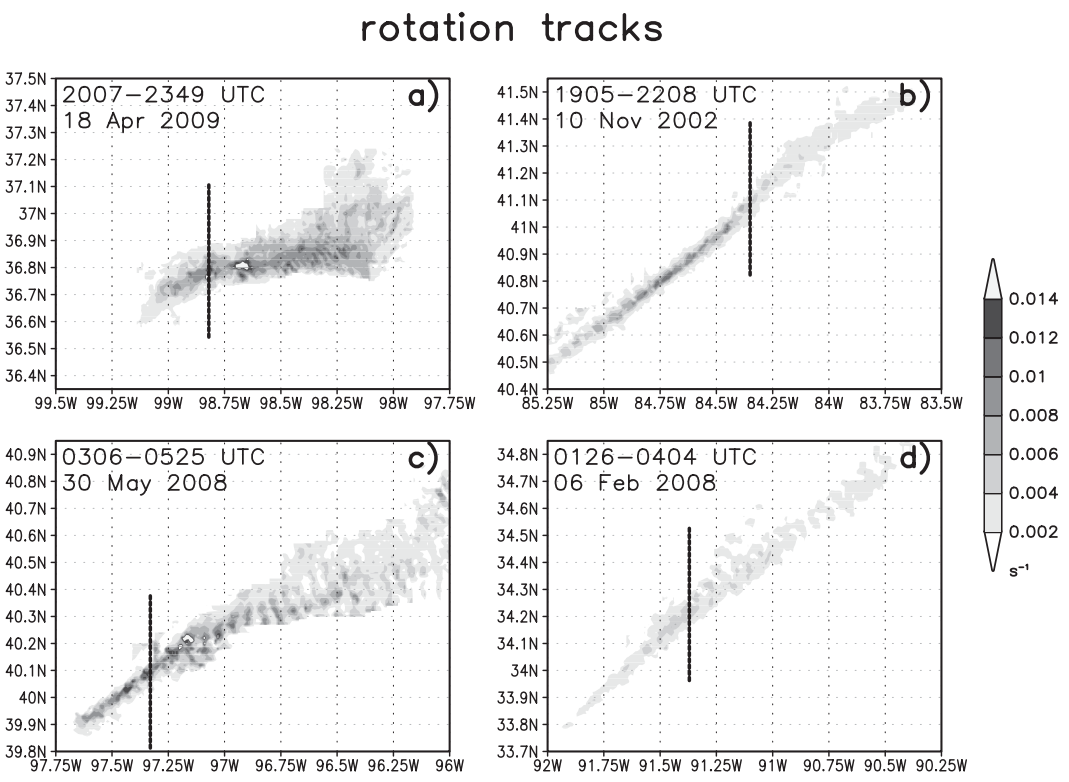

FIG. 10. Maximum azimuthal shear (s^{-1}, shaded as shown) accumulated over time to produce rotation tracks associated with the supercell and merged system from (a) the 18 Apr 2009 WF case, (b) supercell 1 in the 10 Nov 2002 SF case, (c) the 30 May 2008 WF case, and (d) supercell 4 in the 6 Feb 2008 SF case. The vertical dashed black lines indicate the longitude of the merger in each case.

broadening of the circulation that appears to closely follow the merger in a number of the WF cases (e.g., Figs. 12a–d and 12e–h). As the diameter between the maximum inbound and outbound winds increases, the azimuthal shear (e.g., vertical vorticity) decreases. The comparatively broad postmerger circulations were generally observed north of the bow, collocated initially with the S-shaped echo (Figs. 12c,g), and later the reflectivity swirl/comma echo structures (Figs. 12d,h) common to the observed reflectivity evolutions. In most cases this circulation was strongest in the low to midlevels (e.g., at or below 3 km AGL; Fig. 12), consistent with a shift in the maximum azimuthal shear to lower levels postmerger (Fig. 11). Qualitatively, these postmerger circulations appear very similar to the line-end vortices often observed with bow echoes (e.g., Weisman and Davis 1998; Atkins et al. 2004). From the observations it is unclear whether these features facilitate the developing bow echo, or are instead a result of it.

The mechanism responsible for reintensification of low-level rotation later on (e.g., after $t = +30$ min in Fig. 11a and $t = +15$ min in Figs. 11d,e) is less clear. As discussed above, the postmerger circulations in many of the WF cases appeared to be qualitatively similar to line-end vortex structures. However, line-end vortices tend to reside in the midlevels [e.g., 3–6 km AGL; Weisman and Davis (1998); Atkins et al. (2004)], whereas the features in Figs. 11a,c–f become maximized in low levels over time (e.g., below 3 km AGL by $t = 40$ min.). This is more often observed with squall-line mesovortices (e.g., Funk et al. 1999; Weisman and Trapp 2003; Trapp and Weisman 2003; Atkins et al. 2004; Atkins and St. Laurent 2009a,b), which tend to be smaller in scale and focused at lower levels. Figure 13 provides an example of mesovortices associated with one of our cases. Following the merger, the original supercell circulation (labeled SC in Figs. 13a–c) moves rearward relative to the developing bow echo, while multiple mesovortices develop just north of the apex of the bow echo (labeled MV1–MV3 in Figs. 13b–d) and move rearward along a similar path as the remnant supercell circulation. Similar to the initial supercell circulation, several of these mesovortices widen over time, appearing to evolve toward line-end vortices (e.g., MV1 in Figs. 13c–d). Thus, the postmerger low-level maximum in rotation may result from the presence of line-end vortex and mesovortex features, both of which

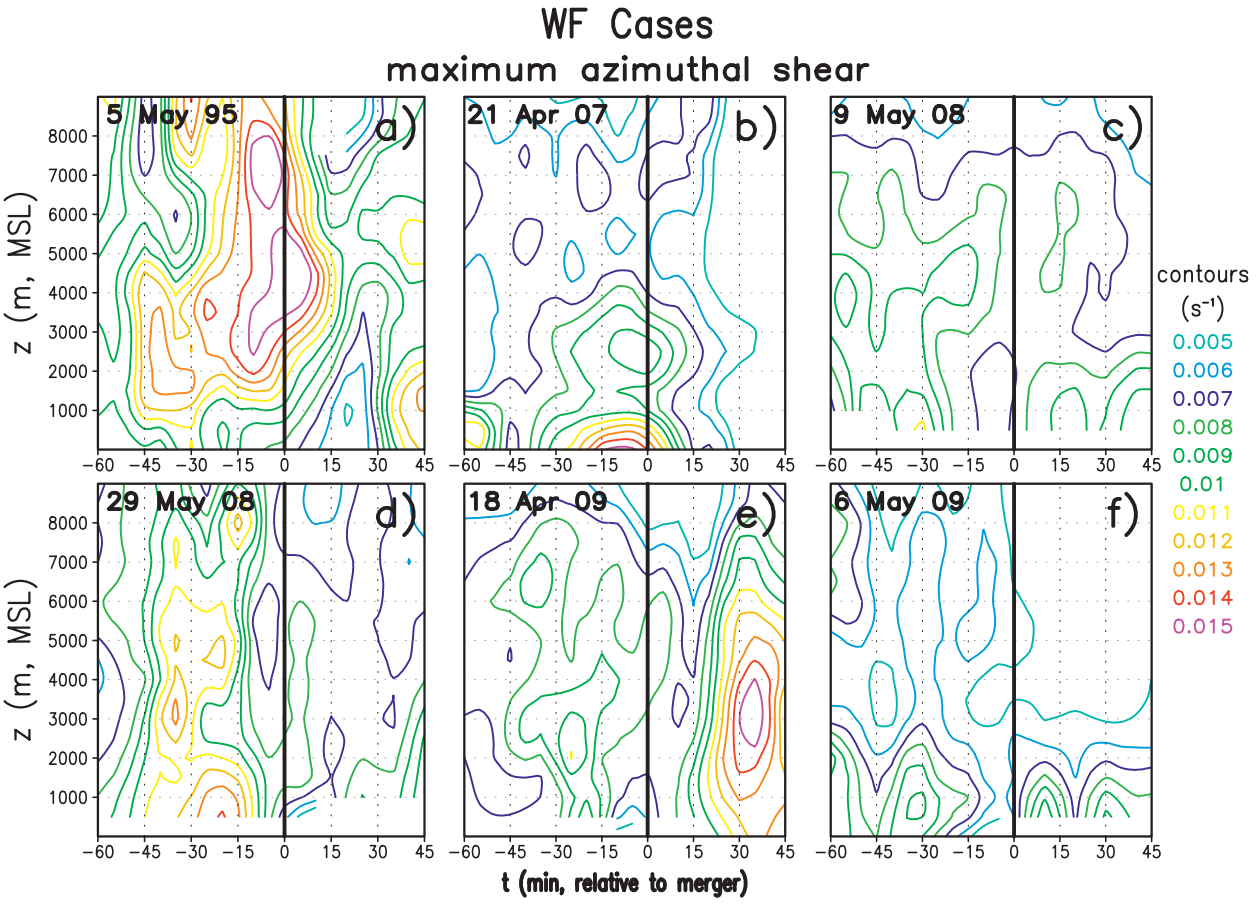

FIG. 11. Time vs height plots of maximum azimuthal shear [contoured, (s^{-1}), as per color scheme on right side of figure] associated with the isolated supercell (premerger) and merged system (postmerger) for the (a) 6 May 1995, (b) 21 Apr 2007, (c) 9 May 2008, (d) 29 May 2008, (e) 18 Apr 2009, and (f) 6 May 2009 WF cases. Time is in a merger-relative framework, with $t = 0$ corresponding to the merger time, which is annotated with a vertical black line.

were present in our cases, and both of which are often observed with bow echoes.

Several common rotational features were also observed in the SF cases; however, these represent a slightly different evolution than that seen in the WF cases. First, in a number of SF events, azimuthal shear is observed to increase prior to the merger at varying depths throughout the troposphere (e.g., Figs. 14b,d,e,f). While this may simply be capturing fluctuations in intensity common to the life cycle of supercell thunderstorms, it is also possible that the squall lines in these cases are altering the local environment in a way that favors storm rotation, as hypothesized by LaPenta et al. (2005). While the present observations are insufficient to ascertain to what extent this may be occurring, it has been well documented that squall lines can perturb the nearby wind and thermodynamic fields (e.g., Lafore and Moncrieff 1989; Nicholls et al. 1991; Weisman and Davis 1998; Fovell 2002; Trier and Sharman 2009; Bryan and Parker 2010), and the impact that such changes may have on nearby storms deserves further consideration in a future study.

A second common feature to these cases, which shares a similarity with the WF cases, is that the strongest rotation generally becomes confined to lower levels (e.g., below 3 km AGL) following the merger (Figs. 14a,b,d,e,f). However, in contrast to the WF cases, there is no significant weakening of the initial rotation prior to the development of this low-level feature. Rather, it appears that the low-level rotation gradually becomes dominant as the mid- and upper-level rotation weakens. As with the WF cases, an analysis of the actual radial velocity data sheds some light on how to interpret this behavior. In many of the SF cases the postmerger circulation does not appear to broaden as much as those in the WF cases (e.g., Figs. 12i–l and 12m–p), which may account for the maintenance of strong rotation following the merger. This is more consistent with the maintenance of an embedded supercell-type feature, as suggested in the EMB reflectivity evolutions.

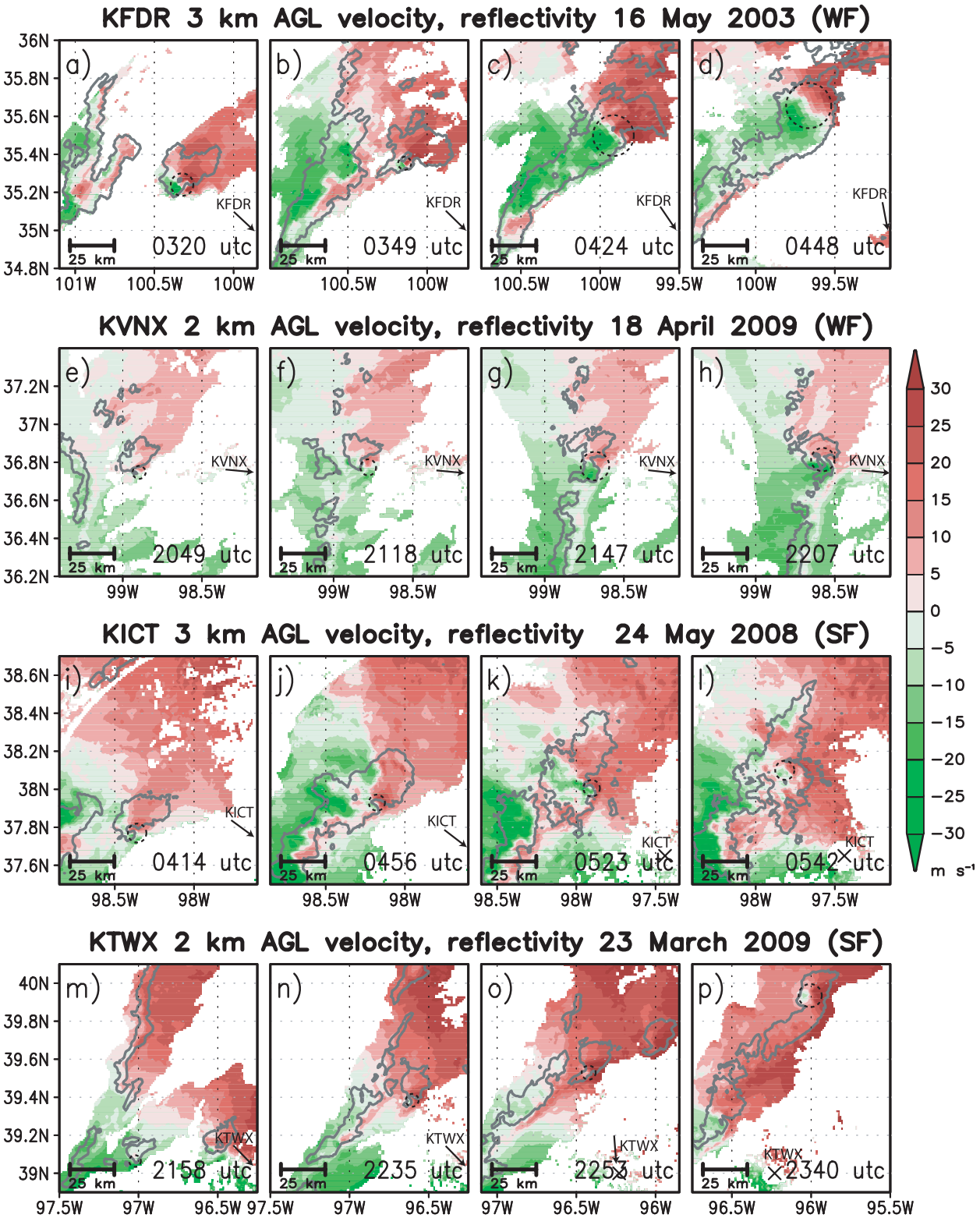

FIG. 12. Constant-height, ground-relative WSR-88D velocity data (m s^{-1}, shaded as shown) and 45-dBZ radar reflectivity contour from (a)–(d) Frederick, OK, on 15 May 2003 at 3 km AGL; (e)–(h) Vance Air Force Base, OK, on 18 Apr 2009 at 2 km AGL, (i)–(l) Wichita, KS, on 25 May 2008 at 3 km AGL, and (m)–(p) Topeka, KS, on 23 Mar 2009 at 2 km AGL. In all panels dashed circles represent approximate diameters of the circulation features initially associated with the premerger supercell. Black arrows point toward the radar location in panels where it is outside the plotting area; otherwise, the radar location is denoted by a black ×. Radar reflectivities from the cases in (a)–(d) and (m)–(p) are also presented in Figs. 9a–e and 9f–j, respectively.

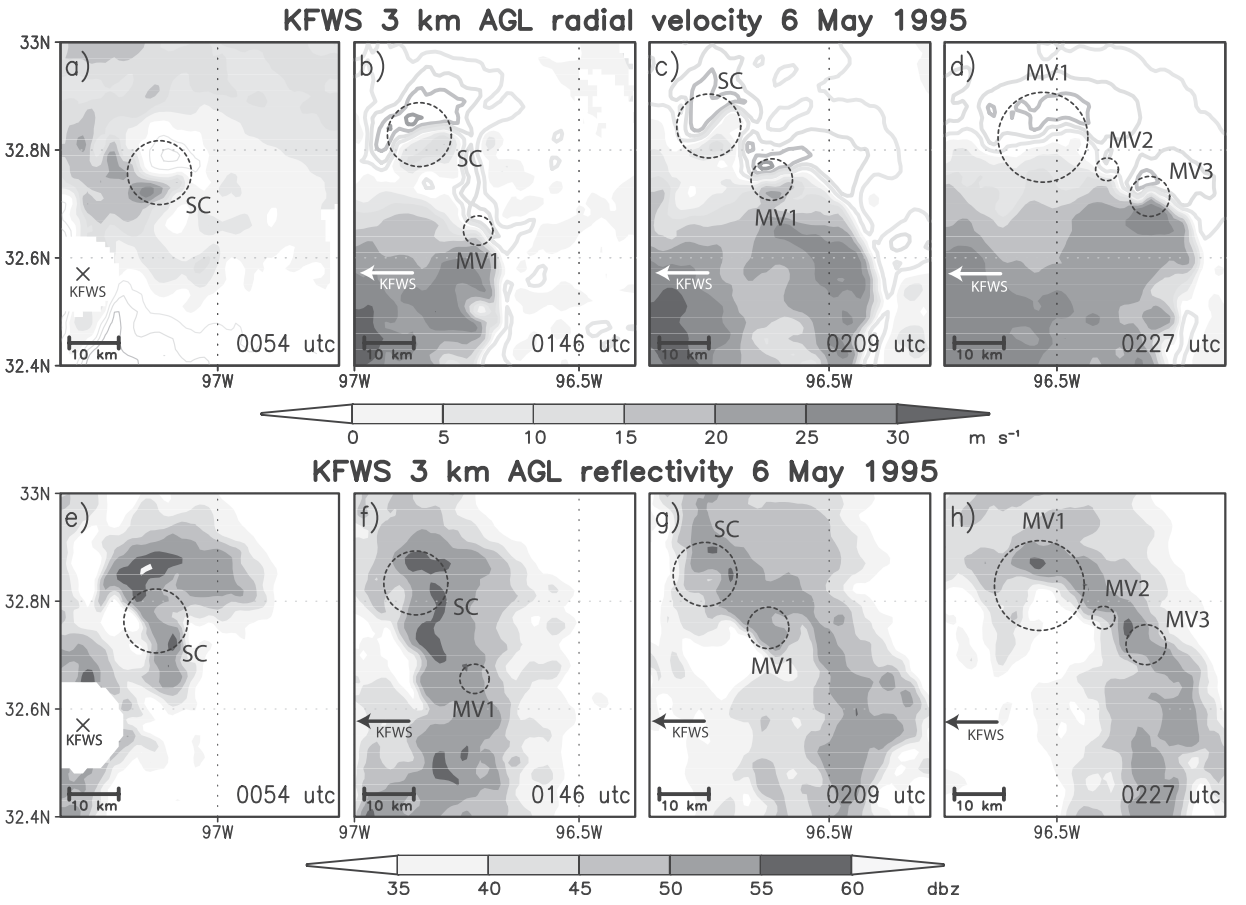

FIG. 13. (a)–(d) Constant-height, ground-relative WSR-88D velocity data [m s^{-1}, positive (outbound) values shaded as shown, and negative (inbound) values contoured using the same color scheme] and (e)–(f) radar reflectivity from KFWS at 3 km AGL from 0054 to 0227 UTC 6 May 1995. In all panels dashed circles represent the approximate diameters of the circulation initially associated with the premerger supercell (labeled SC) and subsequent mesovortices (labeled MV). White (black) arrows point toward the radar location in (b)–(d) [(f)–(h)] where it is outside the plotting area; otherwise, the radar location is denoted by a black ×.

e. Storm reports

As a means of quantifying the impact of squall-line–supercell mergers on severe weather production, we examined storm reports associated with the each of our cases. This includes reports of tornadoes, wind > 25 m s^{-1} ($\sim$50 kt, where 1 kt $= 0.514$ m s^{-1}), and hail > 2.0 cm ($\sim$0.75 in., where 1 in. $= 2.54$ cm) in diameter associated with the isolated supercell(s) and the portion(s) of the squall line involved in the merger(s),[2] and the subsequent merged system(s) in each case. Past studies have revealed drawbacks to the *Storm Data* report database, including inconsistencies and errors in the times and locations associated with some reports (e.g., Witt et al. 1998; Trapp et al. 2006), and an obvious bias toward populated areas [i.e., severe weather is only reported when there is someone around to report it; e.g., Weiss et al. (2002)]. Additionally, wind and hail reports suffer from the drawback that they are recorded as point observations rather than representing a more realistic path or swath of damage, making them less representative of the actual event (e.g., Doswell et al. 2005). In light of this, we attempted to tread carefully in our analysis of the severe storm reports, and the conclusions that we drew from them.

To relate the severe reports to the merger itself, we focused on the reports that occurred within an hour before and after the merger. Since the mergers were observed to take between 20 and 30 min on average (depending on the evolution), we define the "merger" as

[2] Only reports the occurred within 50 km of the portion of the squall line eventually involved in the merger were counted, as in some cases the squall line extended for 10s or 100s of kilometers away from the merger location. This was done subjectively using radar animations to track the section of the squall line eventually involved in the merger backward in time and, generally, was restricted to the time period where the merging supercell was also present.

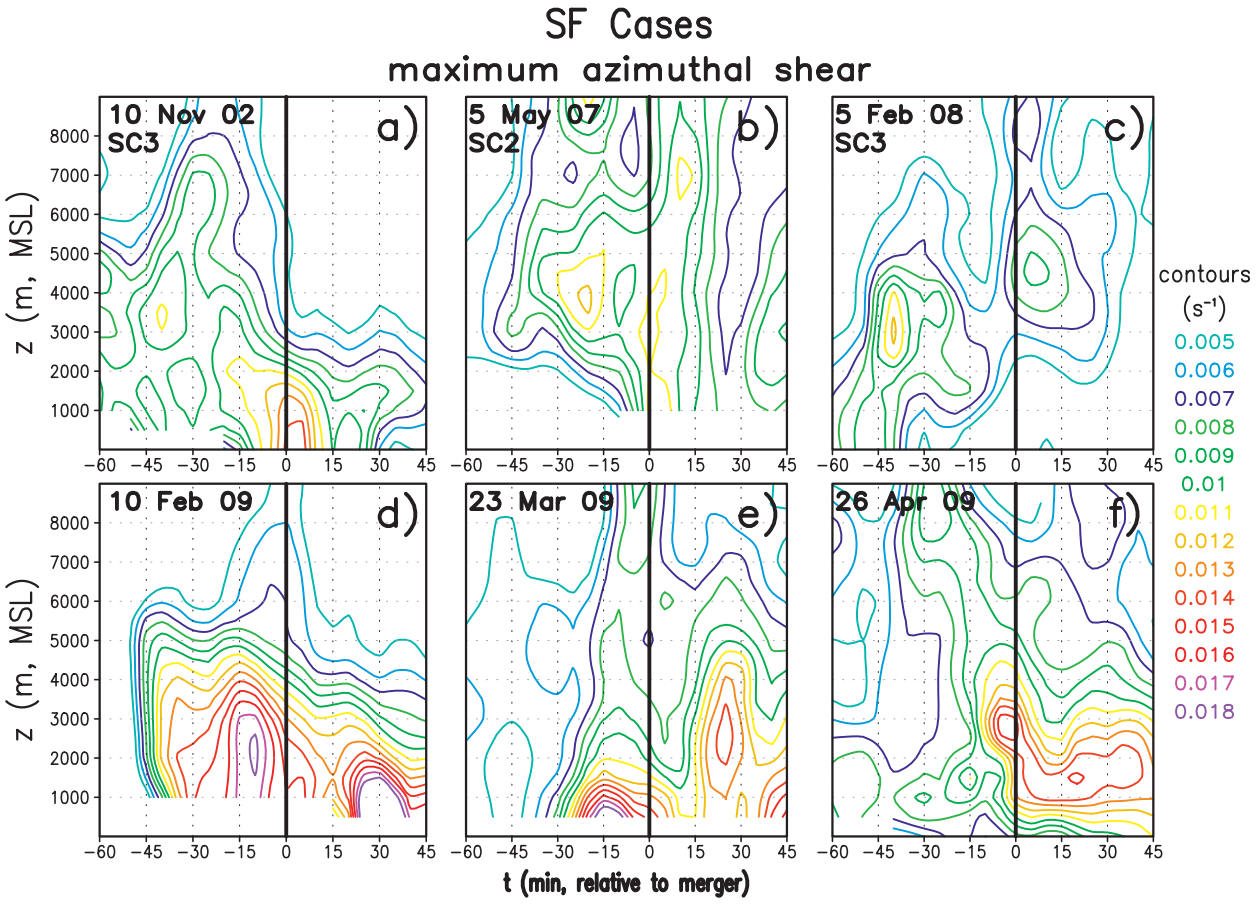

FIG. 14. As in Fig. 11, but for the (a) 10 Nov 2002, (b) 5 May 2007, (c) 5 Feb 2008, (d) 10 Feb 2009, (e) 23 Mar 2009, and (f) 26 Apr 2009 SF cases. SC2 or SC3 in (a)–(c) identify the data as relating to the second or third supercell merger in these cases, as there were multiple.

a 30-min window starting at the time of first observed 40-dBZ radar echo interaction. While it would be tempting to try to make a detailed assessment of severe weather production at a specific time in the storm's evolution, the apparent uncertainty inherent in the storm report dataset precludes such an analysis. Instead, we examined the storm reports in terms of 30-min time windows over the hour before and after merger occurrence. We looked first at the raw reports occurring over this time, to determine the case-to-case variability and gain a general overview of the distribution of reports (plotted in Figs. 15 and 16). Additionally for each case we calculated the fraction of each report type (wind, hail, tornado) that occurred during the merger and each 30-min time bin before and after the merger. These were then averaged across all of the cases reporting severe weather to produce an overall picture of when the largest fractions of severe weather occurred (values presented at the top of each column in Figs. 15 and 16). This method allows for quantified comparison between all of our cases despite substantial ranges in the total numbers of reports (anywhere from 1 to 85 reports) per case.

It is clear from Figs. 15 and 16 that there is a great deal of case-to-case variability in both the WF and SF environments, both in terms of the total numbers of reports, as well as in their distributions relative to the merger. There are, however, some patterns that emerge that appear to differentiate the two environments. In the WF cases, the largest fraction of severe wind reports occurs during the time windows during and just following the merger (Fig. 15a). This is consistent with an increase in damaging straight-line winds that would be expected with the formation of bow-echo structures. In the SF environment, the largest percentage of severe winds also occurs postmerger; however, it is maximized 30–60 min following the merger (Fig. 16a). This too is consistent with the observed storm evolution in these cases, as in many of the SF cases it took longer for the bow-echo structures to emerge (cf. the EMB evolution discussed in section 3c), which suggests a delay in the

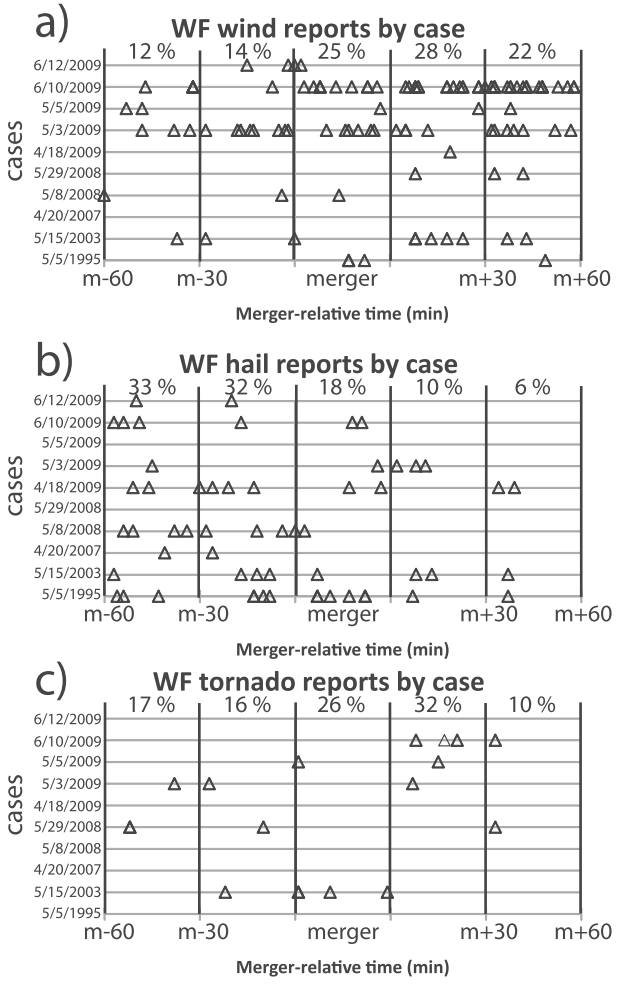

FIG. 15. Reports of (a) severe wind, (b) severe hail, and (c) tornadoes, over time for the WF cases indicated along the *y* axis. The vertical lines denote 30-min time windows, with the middle column (labeled ''merger'') corresponding to the window where the merger occurs. Percentages at the top of each column indicate the average fraction of reports that occurred during that time range, as discussed in the text.

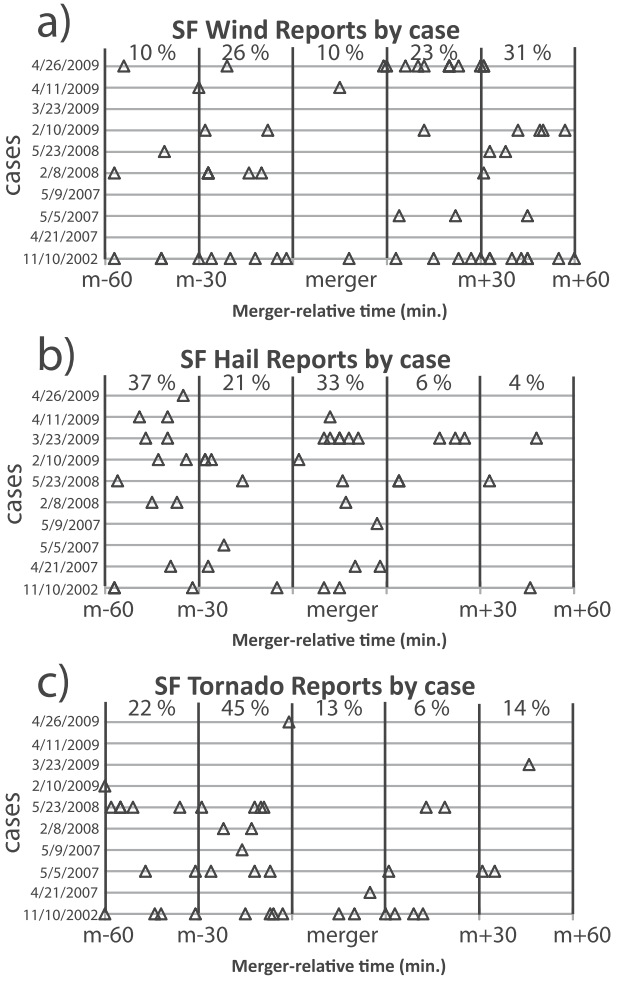

FIG. 16. As in Fig. 15, but for the SF cases indicated along the *y* axis.

onset of severe winds. Also striking was the relative minimum in severe wind reports (10% of the reports for a given case, on average) during the merger itself for the SF cases. This may imply that the merger in some way disrupts the system in the SF cases, leading to a diminished severe weather threat until the bowing features develop later on. For both environments the largest fraction of hail reports occurs prior to the merger, with significantly reduced hail during the postmerger time windows (Figs. 15b and 16b). In most cases these premerger hail reports were associated with the isolated supercells, consistent with past observations of large hail being associated more with isolated supercells than squall lines/bow echoes (e.g., Klimowski et al. 2003; Duda and Gallus 2010).

To compare the present work with several past studies (e.g., Goodman and Knupp 1993; Sabones et al. 1996; Wolf et al. 1996; Wolf 1998) that have investigated the role of squall-line–supercell mergers as a trigger for tornadogenesis, it is of interest to look in detail at the tornado reports associated with these cases. Looking first at the WF environment, perhaps one of the more striking features is the overall dearth of tornado reports, with half of the WF cases recording no tornado reports during the 2-h window centered on the merger (Fig. 15c). However, of the cases where tornadoes were observed, the largest fractions of reports occurred for the time bins during and just after the merger (Fig. 15c). This suggests the possibility of an enhanced tornado threat associated with the merger process. One possible interpretation would be that while tornadoes are clearly a rare phenomenon in the mean WF environment, in individual cases where conditions favor tornadogenesis the merger may play a role in instigating that process.

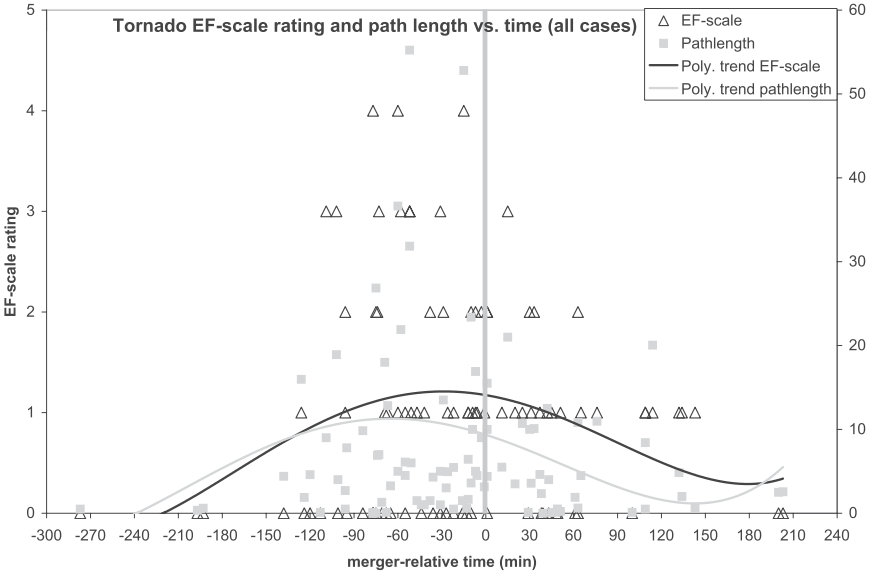

FIG. 17. EF rating (triangles) and pathlength (squares) vs time for tornadoes in all merger cases (WF and SF). The black and gray lines represent a fourth-order polynomial trend line fit to the EF scale and pathlength reports, respectively. The vertical gray line denotes the merger time.

The cases associated with the SF environment produced more tornado reports overall (all but one case produced at least one tornado report; Fig. 16c), which is not surprising given the large 0–1-km SRH values common to this environment (Fig. 6b). However, the largest fractions of reports occur for the time windows prior to the onset of merging (Fig. 16c), and a review of the cases revealed that most of reports were associated with the isolated supercells. Following the onset of the merger, there was a marked decline in the fraction of tornado reports, suggesting a diminished tornado threat (Fig. 16c). Notably, for both environments, the tornadoes that do occur postmerger were generally weaker (rated less than EF2 on the enhanced Fujita scale) and shorter tracked (<10 km) than those that occurred with the premerger supercells (Fig. 17) and in many cases were observed to occur near the ''comma head'' region of the postmerger bow echo (not shown). Taken as a whole, these observations suggest a postmerger tornado threat consistent with past observations of bow-echo tornadoes (e.g., Fujita 1978; Wakimoto 1983; Przybylinski 1995; Atkins et al. 2004; Trapp et al. 2005), as might be expected given the overall evolution toward bowing structures in the cases presented.

4. Conclusions and future work

A radar and RUC analysis based study has revealed two basic environments in which squall-line–supercell mergers occur, one characterized by strong synoptic forcing and strong shear (the SF environment), and the other by weak synoptic forcing and weak-moderate shear (the WF environment). Across these two environments, a spectrum of convective evolutions were observed, generally leading to the development of bow-echo structures following the merger. For cases in the WF environment this was most often characterized by the entire squall line evolving into a large bow echo following the merger (the SSB evolution). In the SF environment, a handful of cases followed an evolution that produced small-scale bowing segments embedded within a larger squall line after the merger (the EMB evolution), while the majority exhibited an evolution best described as a hybrid of the SSB and EMB (the hybrid evolution). Analysis of radial velocity data revealed that the evolution of rotational features during the merger varied between the WF and SF environments as well. In general, an initial weakening of the supercell's mesocyclone was observed in the WF cases, associated with a broadening of the circulation as the merger occurs. This appeared to be qualitatively similar to the development of a line-end vortex associated with the developing bow echo. In the SF cases, strong low-level rotation was maintained and the initial supercell circulation did not broaden as dramatically postmerger, suggesting more of an embedded supercell structure. In both environments, the strongest rotation became concentrated in lower levels after the merger occurred.

A number of past studies have examined cases where the types of mergers discussed in this paper appear to

lead to tornadogenesis. For the present cases, it would appear that the importance of the merger in tornado formation may be linked to the background environment. A larger fraction of tornado reports occurred during or just after the merger in the WF environment, whereas the peak in the SF environment occurred with the premerger supercells. It is important to note that while there appeared to be a link between the merger and tornado production in the WF cases, tornadoes only occurred in 50% of these cases overall. Given the overall rarity of tornadoes in general (e.g., Brooks et al. 2003), this is not all that surprising, but it does underscore that the merger alone is likely insufficient to favor tornadogenesis. Rather, we speculate that in cases where conditions may be favorable for tornado formation, the merger may in some way serve as an instigator. This speculation is lent further credence by our observations of enhanced low-level rotation following the merger for a number of cases in both the WF and SF environments (e.g., Figs. 11 and 14), suggesting that some aspect of the merger appears to favor the development of low-level vertical vorticity.

In addition to the possible role in tornadogenesis, our results also suggest a connection between the merger and straight-line damaging wind reports, with the largest fraction of severe wind reports following the merger in both the WF and SF environments. This is not a surprising result, given that mergers tended to favor the development of bow echoes, which have long been associated with damaging winds (e.g., Fujita 1978). While this is an obvious indication that the portion of a squall line should be monitored for potential severe weather, the degree to which it may be more severe than other portions of the squall line is less clear. In most of the present cases severe weather was also reported along portions of the squall line not involved in the merger or from other nearby storms that did not merge. Unfortunately, the current *Storm Data* reports are insufficient to try to characterize the relative severity of these regions. More detailed damage surveys such as those sometimes performed during field programs would likely be necessary to make such an assessment. Thus, we emphasize that the merger likely represents a location for damaging winds along the squall line, but it may not be the sole location, nor the most severe.

Finally, as has been mentioned throughout this manuscript, the present observations have been used to identify common features related to squall-line–supercell mergers, but have limitations when it comes to revealing the underlying processes responsible for the observed patterns of behavior. To this end, a follow-on study is under way using convection-resolving idealized numerical simulations to delve into the storm-scale processes at work in these types of events. In particular, we are interested in the details of interactions between the squall line's cold pool and supercell's mesocyclone, and how these processes may impact the evolution of low-level vertical vorticity during the merger processes. Additionally, we are hoping to shed some further light on the relative impacts of details such as the location of the merger along the squall line, the premerger storm motions, and the role of the background environment in producing the SSB, EMB, and hybrid postmerger evolutions that have been observed. The results of this work will be presented in a future paper.

Acknowledgments. The authors thank Casey Letkewicz, Matt Morin, and Johannes Dahl of the Convective Storms Group at North Carolina State University for helpful comments and assistance throughout the course of this project. Drs. Sandra Yuter, Gary Lackmann, and Anantha Aiyyer also provided valuable feedback throughout the course of this work as part of the first author's doctoral dissertation committee. Additionally, the insightful comments from two anonymous reviewers greatly enhanced this manuscript. Computational resources and data storage were provided by the Office of Information Technology High Performance Computing at North Carolina State University. We would also like to thank the developers of the WDSS-II software for maintaining and providing this software free of charge for research purposes. This research was supported by NSF Grants ATM-0552154 and ATM-0758509.

REFERENCES

Atkins, N. T., and M. St. Laurent, 2009a: Bow echo mesovortices: Part I: Processes that influence their damaging potential. *Mon. Wea. Rev.,* **137,** 1497–1513.

——, and ——, 2009b: Bow echo mesovortices: Part II: Their genesis. *Mon. Wea. Rev.,* **137,** 1514–1532.

——, J. M. Arnott, R. W. Przybylinski, R. A. Wolf, and B. D. Ketcham, 2004: Vortex structure and evolution within bow echoes. Part I: Single-Doppler and damage analysis of the 29 June 1998 derecho. *Mon. Wea. Rev.,* **132,** 2224–2242.

Benjamin, S. G., and Coauthors, 2004: An hourly assimilation–forecast cycle: The RUC. *Mon. Wea. Rev.,* **132,** 495–518.

Brooks, H. E., C. A. Doswell III, and M. P. Kay, 2003: Climatological estimates of local daily tornado probability in the United States. *Wea. Forecasting,* **18,** 626–640.

Bryan, G. H., and M. D. Parker, 2010: Observations of a squall line and its near environment using high-frequency rawinsonde launches during VORTEX2. *Mon. Wea. Rev.,* **138,** 4076–4097.

Calianese, E. J., J. K. Jordan, E. B. Curran, A. R. Moller, and G. Woodall, 2002: The Mayfest high-precipitation supercell of 5 May 1995—A case study. Preprints, *21st Conf. on Severe Local Storms,* San Antonio, TX, Amer. Meteor. Soc., P3.4. [Available online at http://www.ams.confex.com/ams/pdfpapers/47099.pdf.]

Crum, T. D., and R. L. Alberty, 1993: The WSR-88D Operational Support Facility. *Bull. Amer. Meteor. Soc.,* **74,** 1669–1687.

Davies-Jones, R., J. R. Trapp, and H. B. Bluestein, 2001: Tornadoes and tornadic storms. *Severe Convective Storms, Meteor. Monogr.,* No. 50, Amer. Meteor. Soc., 167–221.

Doswell, C. A., III, and D. W. Burgess, 1988: On some issues of United States tornado climatology. *Mon. Wea. Rev.,* **116,** 495–501.

——, and ——, 1993: Tornadoes and tornadic storms: A review of conceptual models. *The Tornado: Its Structure, Dynamics, Prediction, and Hazards, Geophys. Monogr.,* Vol. 79, Amer. Geophys. Union, 161–172.

——, and J. S. Evans, 2003: Proximity sounding analysis for derechos and supercells: An assessment of similarities and differences. *Atmos. Res.,* **67–68,** 117–133.

——, H. E. Brooks, and M. P. Kay, 2005: Climatological estimates of daily local nontornadic severe thunderstorm probability for the United States. *Wea. Forecasting,* **20,** 577–595.

Duda, J. D., and W. A. Gallus Jr., 2010: Spring and summer midwestern severe weather reports in supercells compared to other morphologies. *Wea. Forecasting,* **25,** 190–206.

Evans, J. S., and C. A. Doswell III, 2001: Examination of derecho environments using proximity soundings. *Wea. Forecasting,* **16,** 329–342.

Finley, C. A., W. R. Cotton, and R. A. Pielke, 2001: Numerical simulation of tornadogenesis in a high-precipitation supercell. Part I: Storm evolution and transition into a bow echo. *J. Atmos. Sci.,* **58,** 1597–1629.

Fovell, R. G., 2002: Upstream influence of numerically simulated squall-line storms. *Quart. J. Roy. Meteor. Soc.,* **128,** 893–912.

French, A. J., and M. D. Parker, 2008: The initiation and evolution of multiple modes of convection within a meso-alpha-scale region. *Wea. Forecasting,* **23,** 1221–1252.

Fujita, T. T., 1978: Manual of downburst identification for project NIMROD. SMRP Research Paper 117, University of Chicago, 104 pp. [NTIS N78-30771/1GI.]

Funk, T. W., K. E. Darmofal, J. D. Kirkpatrick, V. L. DeWald, R. W. Przybylinski, G. K. Schmocker, and Y. J. Lin, 1999: Storm reflectivity and mesocyclone evolution associated with the 15 April 1994 squall line over Kentucky and Indiana. *Wea. Forecasting,* **14,** 976–993.

Gallus, W. A., Jr., N. A. Snook, and E. V. Johnson, 2008: Spring and summer severe weather reports over the Midwest as a function of convective mode: A preliminary study. *Wea. Forecasting,* **23,** 101–113.

Goodman, S. J., and K. R. Knupp, 1993: Tornadogenesis via squall line and supercell interaction: The November 15, 1989, Huntsville, Alabama, tornado. *The Tornado: Its Structure, Dynamics, Prediction, and Hazards, Geophys. Monogr.,* Vol. 79, Amer. Geophys. Union, 183–199.

Johns, R. H., 1993: Meteorological conditions associated with bow echo development in convective storms. *Wea. Forecasting,* **8,** 294–299.

——, and W. D. Hirt, 1987: Derechos: Widespread convectively induced windstorms. *Wea. Forecasting,* **2,** 32–49.

Klimowski, B. A., M. J. Bunkers, M. R. Hjelmfelt, and J. N. Covert, 2003: Severe convective windstorms over the northern high plains of the United States. *Wea. Forecasting,* **18,** 502–519.

——, M. R. Hjelmfelt, and M. J. Bunkers, 2004: Radar observations of the early evolution of bow echoes. *Wea. Forecasting,* **19,** 727–734.

Lafore, J.-P., and M. W. Moncrieff, 1989: A numerical investigation of the organization and interaction of the convective and stratiform regions of tropical squall lines. *J. Atmos. Sci.,* **46,** 521–544.

Lakshmanan, V., T. Smith, K. Hondl, G. Stumf, and A. Witt, 2006: A real-time, three-dimensional, rapidly updating, heterogeneous radar merger technique for reflectivity, velocity, and derived products. *Wea. Forecasting,* **21,** 802–823.

——, ——, G. Stumf, and K. Hondl, 2007: The Warning Decision Support System–Integrated Information. *Wea. Forecasting,* **22,** 596–612.

LaPenta, K. D., L. F. Bosart, T. J. Galarneau, and M. J. Dickinson, 2005: A multiscale examination of the 31 May 1998 Mechanicsville, New York, tornado. *Wea. Forecasting,* **20,** 494–516.

Markowski, P. M., E. N. Rasmussen, J. M. Straka, and D. C. Dowell, 1998: Observations of low-level baroclinity generated by anvil shadows. *Mon. Wea. Rev.,* **126,** 2942–2958.

Mesinger, F., and Coauthors, 2006: North American Regional Reanalysis. *Bull. Amer. Meteor. Soc.,* **87,** 343–360.

Moller, A. R., C. A. Doswell III, and R. Przybylinski, 1990: High precipitation supercells: A conceptual model and documentation. Preprints, *16th Conf. Severe Local Storms,* Kananaskis Park, AB, Canada, Amer. Meteor. Soc., 52–57.

——, ——, M. P. Foster, and G. R. Woodall, 1994: The operational recognition of supercell thunderstorms environments and storm structures. *Wea. Forecasting,* **9,** 327–347.

Nicholls, M. E., R. A. Pielke, and W. R. Cotton, 1991: Thermally forced gravity waves in an atmosphere at rest. *J. Atmos. Sci.,* **48,** 1869–1884.

Nolen, R. H., 1959: A radar pattern associated with tornadoes. *Bull. Amer. Meteor. Soc.,* **40,** 277–279.

Przybylinski, R. H., 1995: The bow echo: Observations, numerical simulations, and severe weather detection methods. *Wea. Forecasting,* **10,** 203–218.

Rasmussen, E. N., and D. O. Blanchard, 1998: A baseline climatology of sounding-derived supercell and tornado forecast parameters. *Wea. Forecasting,* **13,** 1148–1164.

Sabones, M., E. M. Agee, and M. Akridge, 1996: The Pulaski County and West Lafayette, Indiana tornadoes, 26–27 April 1994: A case of supercell (mesocyclone) and squall line bow-echo interaction. Preprints, *18th Conf. Severe Local Storms,* San Francisco, CA, Amer. Meteor. Soc., 746–750.

Sieveking, J. E., and R. W. Przybylinski, 2004: The interaction of an HP supercell thunderstorm and bow echo to produce a prolonged severe wind event in east central Missouri. Preprints, *22nd Conf. Severe Local Storms,* Hyannis, MA, Amer. Meteor. Soc., 7A.5. [Available online at http://ams.confex.com/ams/11aram22sls/techprogram/paper_81818.htm.]

Smith, T. M., and K. L. Elmore, 2004: The use of radial velocity derivatives to diagnose rotation and divergence. Preprints, *11th Conf. on Aviation, Range and Aerospace,* Hyannis, MA, Amer. Meteor. Soc., P5.6. [Available online at http://www.ams.confex.com/ams/pdfpapers/81827.pdf.]

Thompson, R. L., R. Edwards, J. A. Hart, K. L. Elmore, and P. Markowski, 2003: Close proximity soundings within supercell environments obtained from the Rapid Update Cycle. *Wea. Forecasting,* **18,** 1243–1261.

Trapp, R. J., and M. L. Weisman, 2003: Low-level mesovortices within squall lines and bow echoes. Part II: Their genesis and implications. *Mon. Wea. Rev.,* **131,** 2804–2823.

——, S. A. Tessendor, E. S. Godfrey, and H. E. Brooks, 2005: Tornadoes from squall lines and bow echoes. Part I: Climatological distribution. *Wea. Forecasting,* **20,** 23–34.

——, D. M. Wheatley, N. T. Atkins, R. W. Przybylinski, and R. Wolf, 2006: Buyer beware: Some words of caution on the use of severe wind reports in postevent assessment and research. *Wea. Forecasting,* **21,** 408–415.

Trier, S. B., and R. D. Sharman, 2009: Convection-permitting simulations of the environment supporting widespread turbulence within the upper-level outflow of a mesoscale convective system. *Mon. Wea. Rev.,* **137,** 1972–1990.

Verbout, S. M., H. E. Brooks, L. M. Leslie, and D. M. Schultz, 2006: Evolution of the U.S. tornado database: 1954–2003. *Wea. Forecasting,* **21,** 408–415.

Wakimoto, R. M., 1983: The West Bend, Wisconsin, storm of 4 April 1981: A problem in operational meteorology. *J. Climate Appl. Meteor.,* **22,** 181–189.

Weisman, M. L., and C. A. Davis, 1998: Mechanisms for the generation of mesoscale vortices within quasi-linear convective systems. *J. Atmos. Sci.,* **55,** 2603–2622.

——, and R. J. Trapp, 2003: Low-level mesovortices within squall lines and bow echoes. Part I: Overview and dependence on environmental shear. *Mon. Wea. Rev.,* **131,** 2779–2803.

Weiss, S. J., J. A. Hart, and P. R. Janish, 2002: An examination of severe thunderstorm wind report climatology: 1970–1999. Preprints, *21st Conf. on Severe Local Storms,* San Antonio, TX, Amer. Meteor. Soc., 11B.2 [Available online at http://ams.confex.com/ams/SLS_WAF_NWP/techprogram/paper_47494.htm.]

Witt, A., M. D. Eilts, G. J. Stumpf, E. D. Mitchell, J. T. Johnson, and K. W. Thomas, 1998: Evaluating the performance of WSR-88D severe storm detection algorithms. *Wea. Forecasting,* **13,** 513–518.

Wolf, P. L., 1998: WSR-88D radar depiction of supercell–bow echo interaction: Unexpected evolution of a large, tornadic, ''comma-shaped'' supercell over eastern Oklahoma. *Wea. Forecasting,* **13,** 492–504.

Wolf, R., R. Przybylinski, and P. Berg, 1996: Observations of a merging bowing segment and supercell. Preprints, *18th Conf. Severe Local Storms,* San Francisco, CA, Amer. Meteor. Soc., 740–745.